Effects of electron beam irradiation on the electrical properties of III-V semiconductor nanowires

LUND UNIVERSITY

Sobhan Sepehri

Department of Physics

Lund University

A thesis submitted for the degree of

Master of Science in physics

June 2013

Acknowledgements

I would like to express my deepest appreciation and sincere gratitude to my supervisor Claes Thelander for his enthusiasm, patience and sense of humor. His guidance together with his knowledge and constant support helped me during this work. I would also like to thank all my friends and my family. I would never have been able to finish my dissertation without their never ending support, encouragement and love. In addition, I acknowledge, with gratitude, my debt of thanks to the European Commission for the financial support during my studies at Lund University as Erasmus Mundus action 2 lot 8 scholarship.

Abstract

Scanning electron microscopy is widely used in nanowire device fabrication. In spite of the attractive high resolution that scanning electron microscopy provides, it influences the electrical properties of III-V nanowires. In this work, influence of electron beam irradiation on field-effect transistor structures based on InAs, InSb and GaSb nanowires is investigated. It is found that due to modification of surface states upon electron beam irradiation of the nanowires, the electrical conductances of n-type (InAs and InSb) and p-type nanowires (GaSb) are affected. The effects are interpreted as exodiffusion of oxygen ions and detachment of ionic adsorbents by the high energy electron beam, which result in conduction enhancement of InAs and InSb nanowires and degradation of conductance in GaSb nanowires. Results suggest that irradiation of nanowires with acceleration voltage between 5 and 20 kV and electron dose higher than 2600 μCcm^{-2} has the potential to locally modulate charge carriers in nanowires and affect their electrical characteristics.

Contents

Contents iv

List of Figures vi

1 Introduction 1

2 Electron-Sample Interaction and Surface States in Semiconductors 4

2.1 Electron-Sample Interaction 5

2.1.1 Elastic Scattering 5

2.1.2 Inelastic Scattering 5

2.1.3 Irradiation Damage 7

2.2 Simulating the Electron Trajectories 9

2.3 Surface States in Semiconductors 13

3 Device Processing and Measurement Setup 18

3.1 Chip fabrication 18

3.2 Device Fabrication 19

3.2.1 Preparing sample chips 20

3.2.2 Deposition and locating of nanowires 20

3.2.3 Fabricating contacts to InAs and InSb nanowires . 22

3.2.4 Fabricating contacts to GaSb nanowires 23

3.3 Suspending the nanowires 24
3.4 Measurement setup and metrics 26

4 Results **28**
4.1 Effect of beam energy and dose on InAs 29
4.1.1 Charging of SiO_2 back-gate oxide 38
4.2 Irradiation of InSb 41
4.3 Irradiation of GaSb 44

5 Discussion and Outlook **48**

A Reference Chips Fabrication **52**
A.1 First metallization 53
A.2 EBL step and second metallization 53
A.3 UV lithography and third metallization 54

References **57**

List of Figures

2.1 Formation of double layer charge due to irradiation of bulk material. $I_\circ$ is the beam current generated from incident electrons. I_η and I_δ are currents of reflected and secondary electrons, respectively. I_{RIC} is the radiation induced current and $a \times a$ is the size of irradiated area Rau et al. [2008]. 9

2.2 (a) 3 dimensional structure of the sample in CASINO software. Electron trajectories in different regions of the sample in (b) 3D view and in (c) x-z plane. 100000 electron trajectories with 10 kV acceleration voltage inside the sample are illustrating the scattering and penetration depth in different regions. 10

2.3 (a) Energy absorbed by the sample and contour energy lines,(b) distribution of maximum penetration depth of trajectory electrons and maximum penetration depth of electron trajectories escaping the sample and (c) energy distribution of electrons escaping from the surface of the sample.(Data generated from simulating 100,000 electron trajectories with 10 kV acceleration voltage.) 12

2.4 Monte Carlo simulation of electron trajectories (a & b) and maximum penetration depths (c & d) at the two acceleration voltages of (a) 5 and (b) 20 kV inside specimen illustrated in figure 2.2, respectively.(CASINO Simulation with 100,000 number of electrons simulated). 14
2.5 Schematic diagram of arrangement of atom at the surface of a solid. The bulk exposed plane mode (a), the relaxation of surface plane and (c) the reconstruction phenomenon of outermost atomic layers forming the surface.(From Prutton [1975]) 15
2.6 P-type semiconductor energy band diagram at the surface.(After Sze [1985]) 17

3.1 Finalized chips on which the devices are fabricated. The highlighted area is the EBL pattern and the rest is fabricated by UV lithography. 19
3.2 (a) optical microscope image and (b) Scanning electron micrograph of nanowires. These images are used to coordinate the position of nanowires in accordance to the coordination marks on the chip. 21
3.3 Scanning micrographs of (a) InAs, (b) InSb(c) undoped GaSb and (d) p-doped GaSb devices. 24
3.4 (a) Side view of suspension structure and (b) scanning electron micrograph of the fabricated structure and (c) suspended InAs device. 25
3.5 Linear extrapolation of threshold voltage implemented on $I_DS - I_GS$ characteristic at constant drain voltage. Typically the device has a true onset voltage which is different from V_T. 27

4.1 Average resistivity of the nanowires aligned with scanning electron microscopy and optical microscope. 29
4.2 $I_D - V_G$ and transconductance of 3 different devices at $V_D = 10mV$. (a) & (b) are the transfer characteristic and transconductance of the reference parts of the nanowires before and after e-beam irradiation and (c) & (d) illustrates the same characteristics for the irradiated parts, respectively. Different colors correspond to different doses of electron. 31
4.3 Transfer characteristics and transconductances of reference and irradiated parts of InAs nanowires with different doses of 10 kV electron beam, V_D = 10mV. 33
4.4 nanowires irradiated by electron beam of 20 kV at $\mathrm{V_D}$ = 10mV. (a) & (b) and (c) & (d) are the transfer curves and transconductances of reference and irradiated parts, respectively. Different colors correspond to different dosage of electron. 35
4.5 (a)Transfer characteristics and (b) corresponding transconductances of devices irradiated by $10 \times 260\mu\mathrm{Ccm}^{-2}$ dose of electron and 3 different acceleration voltages of 5, 10 and 20 kV. 36
4.6 Average Normalized resistance versus the electron dose at three different acceleration voltages of 5, 10 and 20 kV. The data for 10 and 20 kV have been shifted in dose for clarity. 37
4.7 (a-b) and (c-d) correspond to transfer characteristics and transconductance plots of devices irradiated by 100×260 and $1000 \times 260\mu\mathrm{Ccm}^{-2}$ electron doses with various acceleration voltages, respectively. 39

4.8 (a) $I_D - V_G$ of suspended InAs with their corresponding (b) transconductances. Transfer characteristics of color red, black, green and blue belongs to device A, B, C and D, respectively. 41
4.9 Transfer characteristics and transconductances of InSb nanowires irradiated by electron beam of 10 kV at $V_D = 25$mV with different doses of 10×260, 100×260 and $1000 \times 260 \mu$Ccm^{-2} plotted in red, black and green, respectively. (a) & (b) show the transfer curves and g_m of reference parts and (c) & (d) the transfer characteristics and g_m of irradiated parts. 42
4.10 Atomic force microscopy image of InAs nanowire FET irradiated by $1000 \times 260 \mu$Ccm^{-2} electron of 5 kV. The step around the nanowire is the carbonaceous material formed by long electron exposure. 44
4.11 (a) and (c) are $I_D - V_G$ and (b) and (d) are $g_m - V_G$ of reference and irradiated GaSb nanowires with $V_D = 25$mV, respectively. Different doses of electron with 10 kV energy are used to irradiate the wire and are plotted in different colors. 46

5.1 Schematic illustration of adsorption and desorption of oxygen and water molecules based on the explanation proposed for oxide nanowires Ji et al. [2011] on the surface of n-type and p-type nanowires at different steps of measurement:(i) in air, (ii) in evacuation, (iii) in evacuation chamber of SEM for irradiation and (iv) back to the air again. 50

A.1 Optical microscope image of perfectly aligned micrometer size UV lithography pattern with already fabricated EBL patterns. The contrast around the developed area shows the undercut. 56

Chapter 1

Introduction

III-V Semiconductor nanowires are almost one dimensional nano-structures with unique electronic and optical properties. They have the potential to be used in diverse electronic Li et al. [2006], photonic Yan et al. [2009] and biomedical Cui et al. [2001] applications. Regarding the electrical properties nanowires have come forth as a promising candidate for future electronic devices. Device applications such as high performance transistors Dayeh et al. [2007a], sensors and memories have attracted great interest and attention. Due to large surface to volume ratio, the nanowire surface plays a significant role in its electrical properties. Mobility, (electrical) contact properties and hysteresis can be modified by surface states and charges which change the electrical properties. Uncontrollable charge from absorbents on the surface of the nanowire may affect the conduction of the nanowire by modifying the surface charges and states, local work function Smit et al. [1989] & Eremeev et al. [2012] and band alignment as well as band bending Hu et al. [2010], Ji et al. [2011] & Baier et al. [1986]. In order to fabricate devices using nanowires that have been deposited on a substrate, it is necessary to first locate them. There are two classes of imaging techniques that are available

to probe the nanostructures, focal microscopy and scanning microscopy Kittel [2005]. The focal microscopy consists of a series of lenses to focus the probing particle. Examples of which are optical microscope, scanning electron microscopy (SEM) and tunneling electron microscopy (TEM). In scanned probe technique a very sharp tip is brought within a nanometer of the sample and measures either the tunneling current between tip and sample (with conducting samples), scanning tunneling microscopy (STM), or the atomic force between the tip and the sample, atomic force microscopy (AFM). However, the scanning probe technique is very slow since the tip needs to sweep the whole surface pixel by pixel.On the other hand, optical microscopy is yet not very favorable in many cases because the highest resolution is 200-400 nm. This leaves SEM and TEM as the best options and the most powerful and promising real space probes. Both TEM and SEM are fast and easy to use and have very high ultimate resolutions. Theoretically, TEM at typical acceleration voltage of 100 kV has subatomic resolution. However, due to effects such as lens imperfections it has lower resolution; ~ 0.1 nm is achieved Kittel [2005]. Furthermore, in TEM the electron beam needs to penetrate the sample, which consequently limits its applications. Although SEM has a lower resolution > 1nm than TEM, it is the ideal imaging technique in device fabrication because it is fast, easy, has high enough resolution and does not require transparent samples.

Imaging a sample in SEM adversely affects it in various ways. Consequently, elastic and inelastic scattering of energetic electrons can likely cause various types of damage such as heating and displacement Egerton et al. [2004] & Willardson and Beer [1986]. Charging of insulators like oxides Rau et al. [2008] & Melchinger and Hofmann [1995], formation of a carbonaceous layer due to prolonged electron beam exposure Lopez et al. [1993], and modifying the oxidation rate Akamatsu et al. [1998] are also among the influences that electron beam can possibly have on a

specimen.

Scanning electron microscopy is widely used in device fabrication of nanowires. Nevertheless, the impacts of electron beam on the samples are still not known. In this study the effects of electron beam irradiation on InAs, InSb and GaSb nanowires are investigated. In order to systematically study the electron beam effect, four contacts are fabricated on single nanowires separating them into three areas. These areas are defined as reference, buffer and irradiation parts, figure 3.3, and are each used as a single field effect transistor (FET) by considering the gold metal strips on the wire as source and drain. The heavily doped silicon under the SiO_2 insulator film works as the gate terminal. Transfer characteristics of the nanowire is obtained before and after exposing the nanowire to electron beams of different doses and acceleration voltages. Comparing the transfer characteristics show that upon irradiating the resistance of both InAs and InSb nanowires, which are n-type semiconductors, is reduced whereas for the resistance of GaSb nanowires, which are p-type, is increased. Since the nanowires are deposited on a SiO_2 cap layer it can charge up after irradiating the nanowire by e-beam. The effect of the charging of the oxide layer on the transfer characteristic of the nanowire is investigated by suspending the wire on a metal strip. Formation of the carbonaceous layer after long e-beam exposure is also shown by an AFM image.

The objective of the work is to evaluate the use of using electron microscopy in determining the nanowires coordinates for fabrication purposes. This is done by studying the device characteristics before and after e-beam exposure. For the InAs nanowires the results from optically aligned and very low resolution SEM aligned devices do not show any conclusively significant differences to suggest that one should not use SEM. However, for doses of $2.6 \times 10^3 \mu\text{Ccm}^{-2}$ and higher the effect of electron beam is significant on electrical characteristics of nanowires.

Chapter 2

Electron-Sample Interaction and Surface States in Semiconductors

When a specimen is viewed in scanning electron microscopy, accelerated electrons come into interaction with the sample. Both elastic and inelastic collisions of electrons with the sample take place giving rise to secondary electrons which then comprises the scanning electron micrograph. Upon electron interaction with the sample damages are likely to happen. Simulation of electron trajectories inside a sample as well as energy distribution and maximum penetration depth of electrons are available by an open source program called CASINO. Furthermore, due to large surface to volume ratio of nanowires surface effects are very important in these structures. Thus, a very brief and general overview of the surface states in semiconductors is provided.

2.1 Electron-Sample Interaction

Apart from the useful information that scanning electron microscopy provides, it can adversely affect the surface or bulk structure of a specimen. Upon inelastic collision of electrons with the atomic electrons surrounding the nucleus, electrons are scattered giving rise to secondary electron production which basically creates the SEM image. However, electrostatic deflection of electrons by the coulomb field of the nucleus creates elastic scattering of electrons which leads to electron diffraction patterns and back scattered electron contrast in SEM Egerton et al. [2004]. Due to presence of the hydrocarbons in the SEM chamber, there is a chance of hydrocarbon contamination under the influence of electron bombardment. This carbonaceous layer is visible as a darkened surface and is often formed by prolonged exposure to an electron beam Lopez et al. [1993] & Seiler [1983].

2.1.1 Elastic Scattering

As mentioned before there are two scattering mechanisms when an electron interacts with a sample. In elastic scattering there is no energy loss but a possibility of change in direction up to 180°. The primary electrons are scattered by the positive charge of the nucleus of atoms in the material however; the screening due to atomic cloud around the atom could reduce the effect. The back scattered electrons can have enough energy to exit the top surface of the sample. The number of back-scattered electrons varies with material composition due to dependence of the cross section on atomic number of the specimen.

2.1.2 Inelastic Scattering

In inelastic scattering the kinetic energy is not conserved and the lost energy can lead to slow and fast secondary electrons, inner shell ionization,

phonon and plasmon excitation and Bremsstrahlung radiation. Scattering of loosely bound electrons from valance and conduction band by bombardment with primary electrons generates secondary electrons with energies smaller than 50 eV. For micro imaging of the surface these slow secondary electrons are detected. If the electrons interact with the tightly bound atomic electrons they generate fast secondary electrons which have the significant fraction of the energy of the primary electrons and also deviates from its original trajectory by a substantial angle. Since these fast secondary electrons have greater range and larger deviation angle compared to the slow secondary electrons, they consequently deteriorate the resolution of the SEM.

In inner shell ionization the primary electrons interact with the tightly bound electrons of the inner shell and remove them. The vacancy left can then be occupied by an outer shell electron and the excess energy is lost in the form of photo emission. Inasmuch as these transitions are between specific energy levels inside atoms, the emitted photons have well-defined energies specific of that atom. However, if the excess energy is lost by emission of an outer shell electron instead of a photon, an Auger electrons is released. Such electrons will also have well defined energies specific to the atoms in sample.

In Bremsstrahlung the primary electrons interact with the charges in the sample and change their trajectory. Whenever there is a change in the trajectory of an electron a photon is emitted. These photons can have energies from zero to the energy of the incident beam. The number of emitted photons with specific energy reduces by increasing the acceleration voltage. In addition, the passing electrons in the material set off collective oscillation of free electrons which consequently deviates the primary electrons from its original trajectory. Last but not least in the list of inelastic scattering is the scattering of primary electrons due to collective vibration of atoms in crystal structure. These deviation are

very small and the energy loss is of the orders of one tenth of electron volt.

2.1.3 Irradiation Damage

There are different ways that an electron beam encountering a sample during microscopy could adversely affect it Melchinger and Hofmann [1995].

Atomic Displacement Upon conservation of energy a deflected electron in the field of a single atomic nucleus must transfer some amount of energy. This energy loss is considerable for high incident electron energy and low atomic mass number materials. If the energy loss exceeds the displacement energy which is minimum energy to permanently displace an atom in crystal structure, scattering can displace the nuclei to interstitial positions. However, the acceleration voltages used in SEM are too low to induce any dislocation in atomic structure. The specimen can be vulnerable to displacement in TEM with acceleration voltages higher than 100 kV Melchinger and Hofmann [1995].

Electron-beam Sputtering Since surface atoms do not necessary need to be squeezed into interstitial sites and are free to leave the surface of the specimen they require lower energies to leave the sample. Therefore, high-angle elastic interaction of the beam lying on the surface atoms might provide the energy and dislodge them. Nevertheless, due to low energy and current density of the beam, it is unlikely to have sputtering induced damage in scanning electron microscope.

Heating Local temperature could rise due to transfer of energy in inelastic collision of incoming electrons with atomic electrons in a speci-

men. The heat flow generated by scanning electron microscopy in a bulk material is radial which leads to relatively small temperature rise. Heating effects are troublesome in organic material. A thin film of organic specimen examined in SEM of low acceleration voltage (up to 2 kV) could reach temperature of a few hundred degrees since the heat transfer is two dimensional and the electron penetration depth is less than the film thickness which leads to depositing all of the beam energy inside the film.

Electrostatic Charging Charging of insulating samples such as polymers, ceramics and biological materials due to both elastic and inelastic scattering is accompanied by the termination of surface potentials and strong electric fields in probed regions of target. Recently it has been shown that a thin positive charge layer is formed as a result of secondary electrons escape, while capture of primary electrons by deep defect centers bring about a thick negative charge layer. Figure 2.1 illustrates the schematic diagram of double layer charge. A region of $a \times a$ is irradiated by the electron with current $I_\circ$. Primary electrons reflected from depth of $R_\circ/2$ corresponding to current $I_{\circ\eta}$, where η is electron emission coefficient, leaving a negative charge in the sample. Secondary electrons are also emitted from the thin film layer at 3λ, λ is the mean free path of secondary electrons, corresponding to current $I_\circ\delta$, where δ is the secondary electron emission coefficient, leaving positive charge of $I_\circ\delta t$ at the surface (t is the irradiation time). The electric field generated between these two charge layers separates nonequilibrium charge carriers and generates irradiation induced currentI_{RIC} Rau et al. [2008] & Melchinger and Hofmann [1995].

It is also known that polymerization of hydrocarbon molecules on the surface of the specimen due to electron beam irradiation forms a

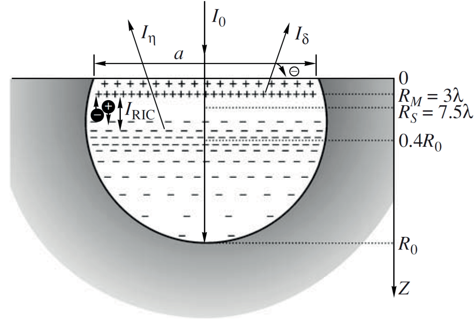

Figure 2.1: Formation of double layer charge due to irradiation of bulk material. $I_\circ$ is the beam current generated from incident electrons. I_η and I_δ are currents of reflected and secondary electrons, respectively. I_{RIC} is the radiation induced current and $a \times a$ is the size of irradiated area Rau et al. [2008].

contamination. These polymers have low vapour pressure and low surface mobility therefore the beam induced contamination thickness increases. The hydrocarbon source for polymerization is provided by diffusion of hydrocarbons along the surface of the specimen Lopez et al. [1993].

2.2 Simulating the Electron Trajectories

Simulation of the passage of electrons through the sample is important for general understanding of relevant mechanisms in the samples studied. To preform this simulation an open source program known as CASINO has been used. CASINO is a simulation tool and its name is derived from "monte CArlo SImulation of electroN trajectory in sOlids" Drouin et al. [2007]. CASINO is specially designed to model low energy electron beam interaction with thin films samples in scanning electron microscopy. In order to perform a simulation a geometric representation of the desired

sample structure is necessary. 3D sample modeling of our structure has been created by simply combining different 3D shapes and planes defined in specific position, orientation and size. Figure 2.2 shows the screen shot of CASINO of the 3D model of the sample.

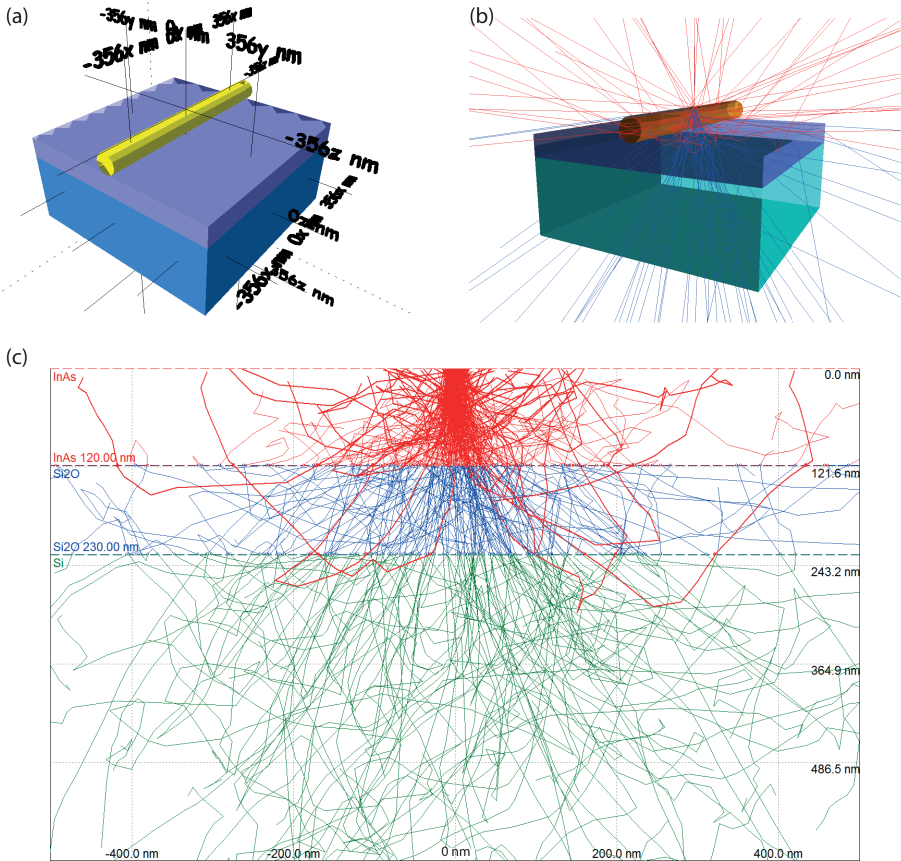

Figure 2.2: (a) 3 dimensional structure of the sample in CASINO software. Electron trajectories in different regions of the sample in (b) 3D view and in (c) x-z plane. 100000 electron trajectories with 10 kV acceleration voltage inside the sample are illustrating the scattering and penetration depth in different regions.

The trajectory of the electrons inside the sample is calculated as follows: In the Monte Carlo method random numbers and probability distributions are used to represent physical interactions and subsequently the electron trajectory, and an electron trajectory is treated as a discrete elastic scattering event. The initial position and energy of the electrons are set by the user as electron beam parameters of the microscope. The electrons are then impinged on the sample and a random number following a probability distribution is used to distribute the distances, obtained from total elastic cross sections, between two successive collisions. Another random number determines the elastic scattering angle using the differential elastic cross section. Keeping the electron direction at the boundary while terminating the electron segment, a new segment is randomly generated using the new material properties. This method is based on Markov process which assumes the past events do not affect the new ones. This process is continued until the electrons either leave or trap inside the sample Demers et al. [2011].

Figure 2.3 demonstrates the details of different distributions for the 3D model illustrated in figure 2.2. The diameter of the InAs nanowire is 120 nm, placed on a heavily doped Si substrate with 100 nm SiO_2 cap. The simulation has been carried out using 100,000 electrons of 10 KeV energy. Figure 2.3(a) displays the contour plot of energy absorption in the sample. Distributions of (b) both maximum penetration depth of electrons in the sample and the maximum penetration depth of electrons escaping the sample surface and (c) the energies of backscattered electrons are also shown in figure 2.3.

A combination of elastic and inelastic scattering inside the specimen limits the penetration depth of electrons. Therefore, the volume of the interaction is affected by the beam energy, angle of incidence together with the atomic number and the density of the specimen. Shape and maximum depth of the interaction volume is influenced by atomic num-

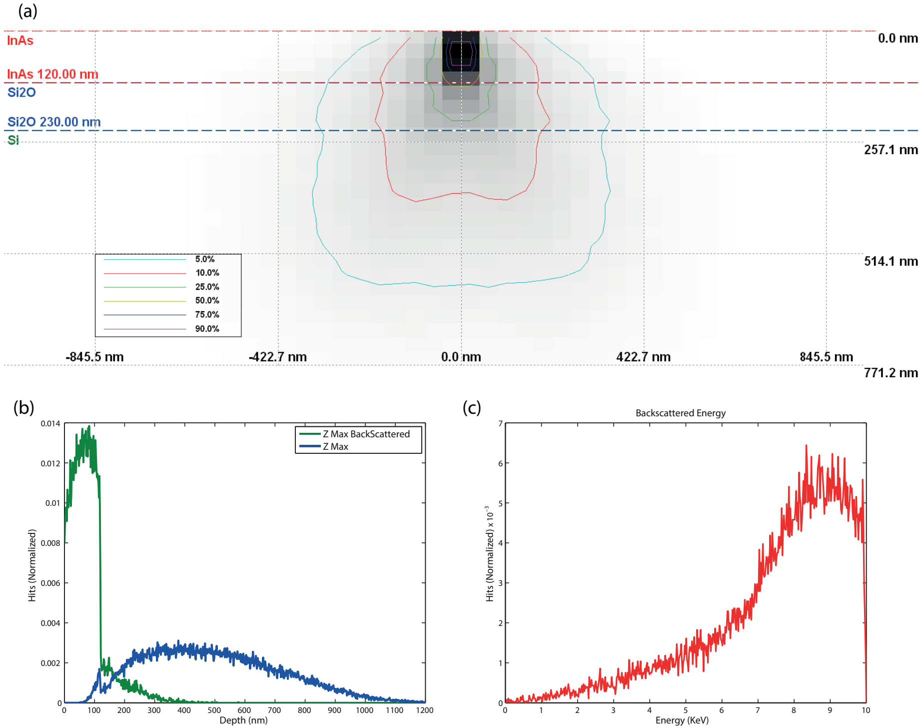

Figure 2.3: (a) Energy absorbed by the sample and contour energy lines,(b) distribution of maximum penetration depth of trajectory electrons and maximum penetration depth of electron trajectories escaping the sample and (c) energy distribution of electrons escaping from the surface of the sample.(Data generated from simulating 100,000 electron trajectories with 10 kV acceleration voltage.)

ber and energy of the incident electrons. In materials of high atomic number there are more elastic scattering and electrons tend to deviate form the initial direction with greater angles. Higher energy electrons do not affect the shape of the interaction volume but penetrate to greater depths. Figure 2.4 illustrates different scattering and penetration depths for electrons of 5 and 20 KeV in the sample.

2.3 Surface States in Semiconductors

The surface of bulk crystalline solids are defined as the top few atomic layers, typically the first three. The surface is expected to have a different properties than the bulk material depending on how the atoms are forming the surface structure. The surface can be either reconstructed or unreconstructed. When the outermost atomic layers are disturbed and rearranged symmetrically different from the bulk, the surface is called reconstructed. Clearly the unreconstructed surface keeps the atomic arrangement of the bulk solid however; they can be bulk exposed plane or relaxation surface. In bulk exposed plane the atomic arrangement is in registry with the bulk solid and are not disturbed from their bulk equilibrium positions. On the other hand, in relaxation process there is a deviation in bulk lattice spacing forming a selvedge Prutton [1975], figure 2.5. The surfaces are of great importance and interest because of a variety of important processes happening there. Adsorption of species to the surface for example can be classified into physiosorption and chemisorption based on the the energy of the bonding Madou and Morrison [1989]. Physiosorption can be considered as a dipole-dipole interaction of polarized molecule approaching the surface and weakly bonding to the surface. Chemisorption, on the other hand, has a stronger chemical bonding energy and relocates the surface atoms inducing adatom surface states which consequently cause band bending Monch [2010].

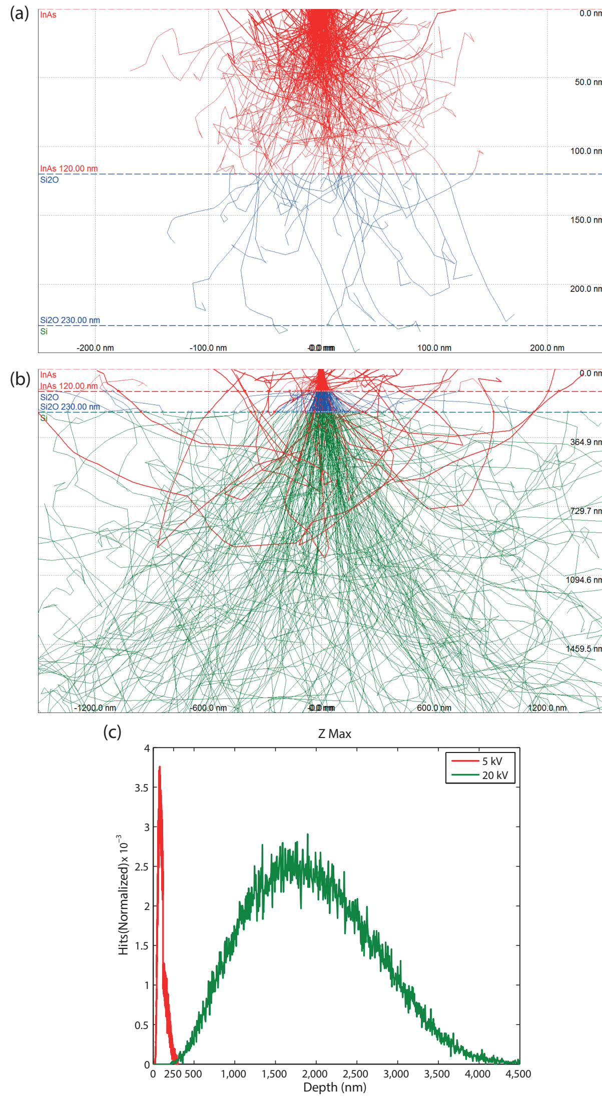

Figure 2.4: Monte Carlo simulation of electron trajectories (a & b) and maximum penetration depths (c & d) at the two acceleration voltages of (a) 5 and (b) 20 kV inside specimen illustrated in figure 2.2, respectively.(CASINO Simulation with 100,000 number of electrons simulated).

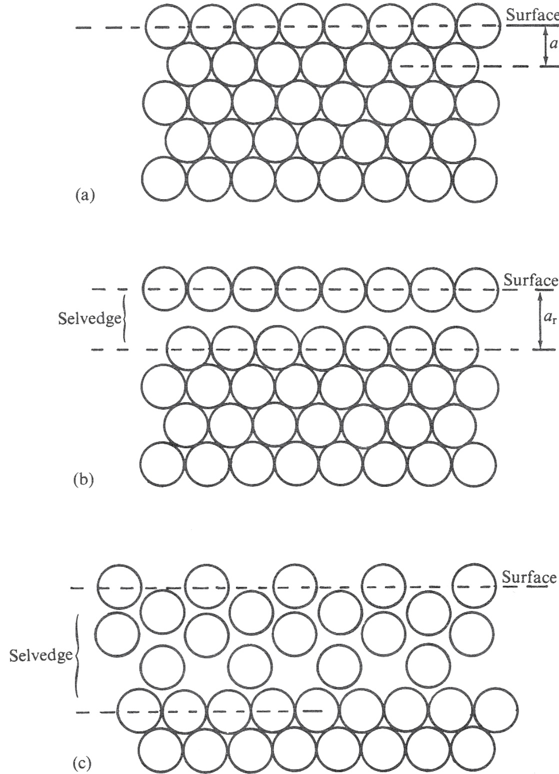

Figure 2.5: Schematic diagram of arrangement of atom at the surface of a solid. The bulk exposed plane mode (a), the relaxation of surface plane and (c) the reconstruction phenomenon of outermost atomic layers forming the surface.(From Prutton [1975])

To shed light on how surface properties are related to their composition and structure one needs to look into the work function and physical factors contributing to it. Work function is the energy difference between a most loosely bound electron inside the solid and an electron at rest in vacuum, more than 100Å in metals. The depth of attractive potentials for the conduction band determines the work function. On the other

hand, the arrangement of positive ions and their type contributes to the depth of attractive forces since it is a bulk property Prutton [1975] & Kittel [2005]. The depth of attractive potential is changed at the surface due to specific surface contributions. There are two mechanisms contribution to this change: *image charge* and *surface double layer*. The former is the classical image charge of opposite sign attracting the charge outside a conductor and it is placed at the position of optical image of that charge. However, it is negligible beyond $10-100$ nm and closer than 0.1 nm a quantum description is necessary. The double layer is formed due to unbalance electron distribution with respect to ions around atoms at the surface. Lack of atoms in one side of the surface creates an asymmetry. This double layer charge makes the working function sensitive to both the crystal orientation of the surface and contamination. Contaminations with different affinities affect the working function differently by modifying the double layer charge. Crystallographic faces exposed at the surface creates different positive and negative charge distributions at the surface due to various number and orientation of core atoms at different faces Prutton [1975].

Schrodinger's equation for a bulk solid with periodic potential has no travelling wave solution however; at the surface where the periodicity is broken travelling wave solutions are sought and they form electronic states with energies in the forbidden gap between valence and conduction band. These solutions, known as surface states, are waves which can only travel parallel to the surface and be localized there. The surface states may be occupied or vacant which can affect the local equilibrium concentrations of holes and electrons. Therefore, the chemical potential should be shifted according to the band edges. However, due to independence of chemical potential from position in equilibrium system the energy band diagrams must bend. In another words, charges at the surface create a penetrating electrostatic field inside the solid which in turn cause a vary-

ing electrostatic potential from the surface to the interior of the solid leading to distortion of the band structure. Figure 2.6 illustrates the band diagram of a p-type semiconductor at the surface. The electrostatic potential ψ is considered to be zero inside the semiconductor. At the surface $\psi = \psi_s$ with ψ_s being the surface potential. The electron and hole concentration in semiconductors are exponential functions of energy difference $q\psi - q\psi_B$, where $q\psi_B$ is the energy difference between the intrinsic and Fermi energy levels. Bands bend upward and downward by negative and positive surface potentials, respectively. If $\psi_s > \psi_B$ the surface is inverted and electrons will accumulate in the conduction band Sze [1985].

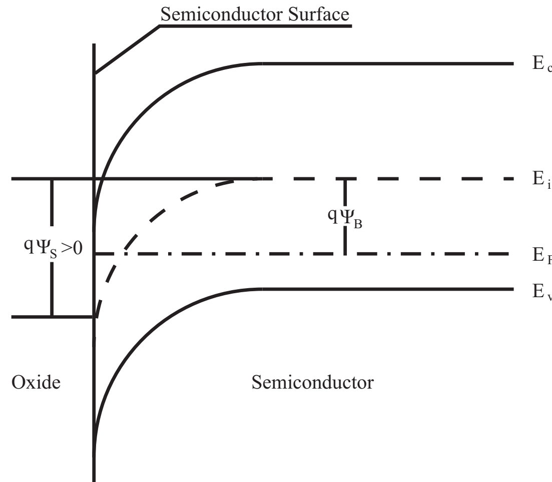

Figure 2.6: P-type semiconductor energy band diagram at the surface.(After Sze [1985])

Chapter 3

Device Processing and Measurement Setup

In this chapter the device fabrication and measurement techniques are explained in details. The fabricated devices are placed on chips which are made out of a heavily doped Si wafer. The whole process of producing the chips and fabricating the devices from them are described here. Figure 3.1 shows a typical chip on which the devices are fabricated.

3.1 Chip fabrication

The chips that are used for device processing during this project are delicate items of heavily doped Si substrate with gold metal covering the back side as a back gate. This wafer is capped with 100 nm of SiO_2 dielectric. Fabricating these chips require electron beam lithography, UV lithography, physical vapor epitaxy, spin coating and lift off. Details of the processing are explained in Appendix 1.

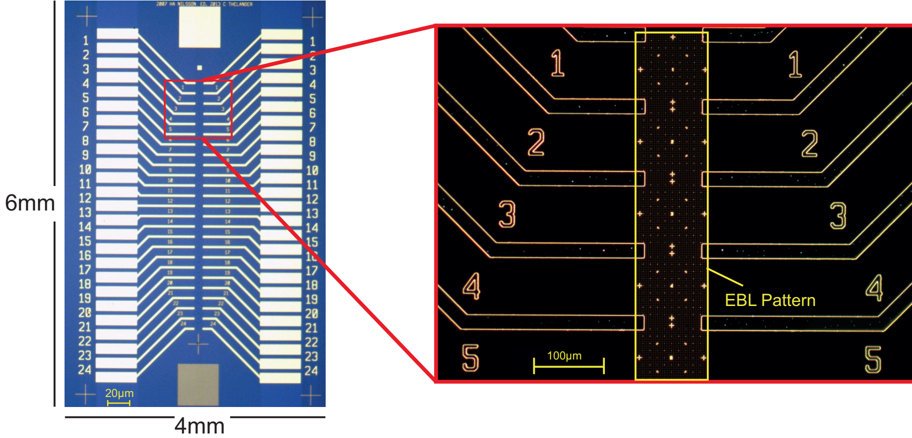

Figure 3.1: Finalized chips on which the devices are fabricated. The highlighted area is the EBL pattern and the rest is fabricated by UV lithography.

3.2 Device Fabrication

Fabricating devices based on nanowires is a sensitive process being conducted in a ISO 7 clean room to avoid particle contamination. The process comprises the following steps and are explained in details:

- Preparing sample chips
- Deposition and locating of the nanowires
- Fabricating the contacts

The processing steps are quite similar for both InAs and InSb nanowires. However, the contact materials and etching steps for GaSb are entirely different and explained accordingly.

3.2.1 Preparing sample chips

Scribed chips need to be cleaned before proceeding with the rest of the processes. To clean the chips they are soaked into Acetone for 5 minutes following sonic bath at low power to remove any particle from the post processes including the scribe. They are then rinsed in IPA and carefully blown dried by Nitrogen gas. The samples are then baked at 120 ℃ for dehydration. Preforming an oxygen plasma ashing for 60 seconds etches away any remaining organic residues from the surface by removing the ash created by combination of reactive species with the remained photoresists on the surface.

3.2.2 Deposition and locating of nanowires

To deposit the nanowires from the growth samples to the chips, a clean room tissue cut into a sharp form is used. Nanowires are picked by the sharp tip of the tissue from the growth sample and transferred to the chip by simply touching it within the EBL pattern. The position of the nanowires on each gap of the chip is investigated in optical microscope or scanning electron microscope. Since it is not known whether determining the coordinates of the nanowires with SEM has any effect on them or not, both optical and SEM methods are implemented. Figure 3.2 shows optical microscope and scanning electron microscopy images of nanowires. Locating a single nanowire by optical microscope can sometimes be a challenge since it is difficult to make distinction between a single nanowire and two attached ones. Consequently, the yield of having single nanowire devices by the use of optical microscope is lower than SEM.

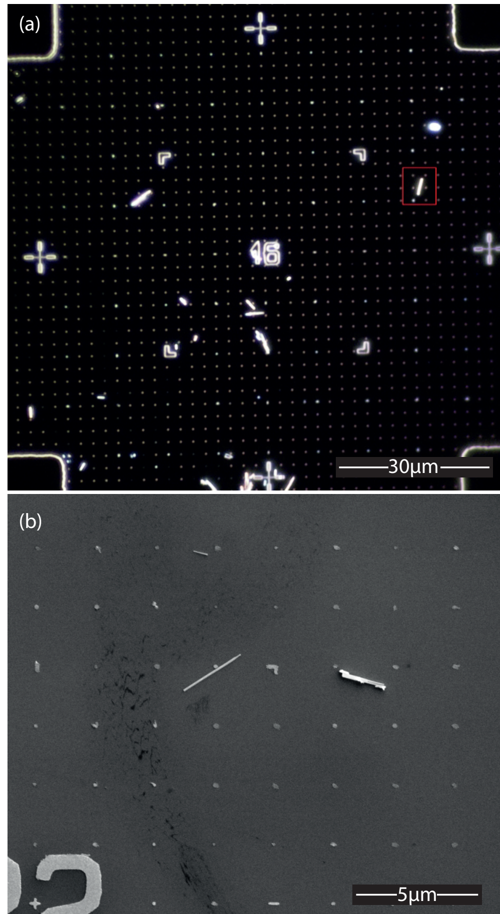

Figure 3.2: (a) optical microscope image and (b) Scanning electron micrograph of nanowires. These images are used to coordinate the position of nanowires in accordance to the coordination marks on the chip.

3.2.3 Fabricating contacts to InAs and InSb nanowires

In order to fabricate contacts, electron beam lithography is used. PMMA[1] is spin coated by the following recipe and baked on hot plate at 180 ℃ for 10 minutes.

- speed up for 3 seconds up to 500 rpm
- spin for 60 seconds at 5000 rpm

According to the data sheet provided by MicroChem [2] the final thickness of the PMMA should be around 2000 Å. The contact pattern are written using EBL Raith 150 using a 20 KV electron beam and 10 μm aperture size. The beam current was measured on the system and the area dose of 260 μCcm^{-2} was applied. Submersing the exposed sample into a 1:3 solution of MIBK in isopropanol (IPA) for 60 seconds at room temperature and rinse in IPA to stop the development gives a desirable resolution. Since PMMA is a positive resist the exposed areas will be dissolved in MIBK. To make sure that there are no residues of the resist in the pattern the scums from the dissolved areas are removed by preforming oxygen plasma ashing for 45 seconds.

Right before the metallization step the oxide on the surface of the nanowires needs to be etched. Submerging the sample into a 1:20 diluted solution of ammonium polysulphide NH_4S_x in deionized water for 60 seconds at 40 ℃ etches the native oxide off the surface of the nanowires and passivates the surface with sulfur atoms. Sulfur pins the Fermi level inside the conduction band and leads to a better contact to the nanowires Thelander et al. [2004]. To remove the ammonium polysulphide solution off the sample it is rinsed into deionized water and then gently blown dried by Nitrogen gas. Titanium and gold films are deposited using

[1] Polymethyl methacrylate.

[2] MicroChem Coorporation, Newton, Ma, USA.

physical vapor deposition systems. The deposition rates for titanium and gold were kept around 2-4 Åand 5-10 Å, respectively. Titanium is used as a sticking layer since gold does not have a good adhesion to the substrate. Nickel can be used instead of titanium however; it diffuses into the nanowire at high temperatures and possibly due to local heating under e-beam irradiation. Last but not the least is the lift-off process. After the metallization the sample is submerged in acetone at 70 ℃ for 15 minutes to remove the extraneous pieces of metal film. Flushing the Acetone with pipette over the submersed sample speeds up the lift off process. It is then rinsed in IPA and blown dry by lightly applying N_2 gas.

The same procedure applies to InSb wires. However, NH_4S_x etches InSb and its oxide faster than InAs. Therefore, the recipe of ammonium polysulphide NH_4S_x solution is attenuated accordingly to dilution of 1:40 with water in which the wires are submerged for 60 seconds at a closely monitor temperature of 40 ℃. Micrographs of contacted InAs and InSb nanowires are illustrated in figure 3.3 (a) & (b), respectively.

3.2.4 Fabricating contacts to GaSb nanowires

The MOCVD grown GaSb nanowires are shorter than the InAs nanowires. Thus, instead of having four metal contacts on the nanowires, two contacts are used. The fabrication process for GaSb nanowires are quite the same as InAs except the etching and metallization. p-doped GaSb nanowires are etched by buffered hydrogen fluoride (BHF) for 5 seconds after which it is submerged in water to stop the etching and blown dry by slightly applying N_2 gas. The metallization is the same as for InAs nanowires and consists of 20 nm thick film of titanium and 80 nm thick layer of gold. On the other hand, undoped GaSb wires are etched by hydrochloric acid (HCl) for 20 seconds following a submerse in water. The metal film deposited is solely 100 nm thick film of palladium. Fig-

ure 3.3 (c) & (d) shows final devices of both undoped and p-doped GaSb nanowires, respectively.

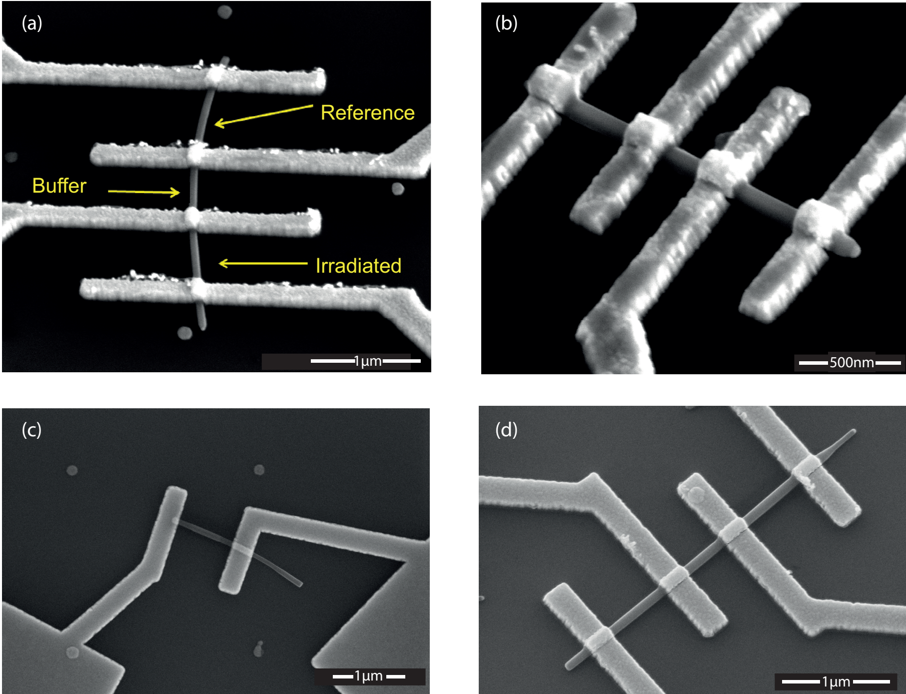

Figure 3.3: Scanning micrographs of (a) InAs, (b) InSb(c) undoped GaSb and (d) p-doped GaSb devices.

3.3 Suspending the nanowires

To shed light on the effects of having the SiO_2 dielectric underneath the nanowires, we have tried to suspend the nanowires on stripes of gold, which could also be used as a local back gate. Here the fabrication is explained whereas the results of having a suspended structure is discussed in the next chapter. The suspension structure consists of two parts with

different height. The source and drain are 80 nm high and the local gate which is supposed to be between the source and drain is 60 nm high. Figure 3.4 (a) shows a side view of the suspension structure and (b) a micrograph of fabricated structure.

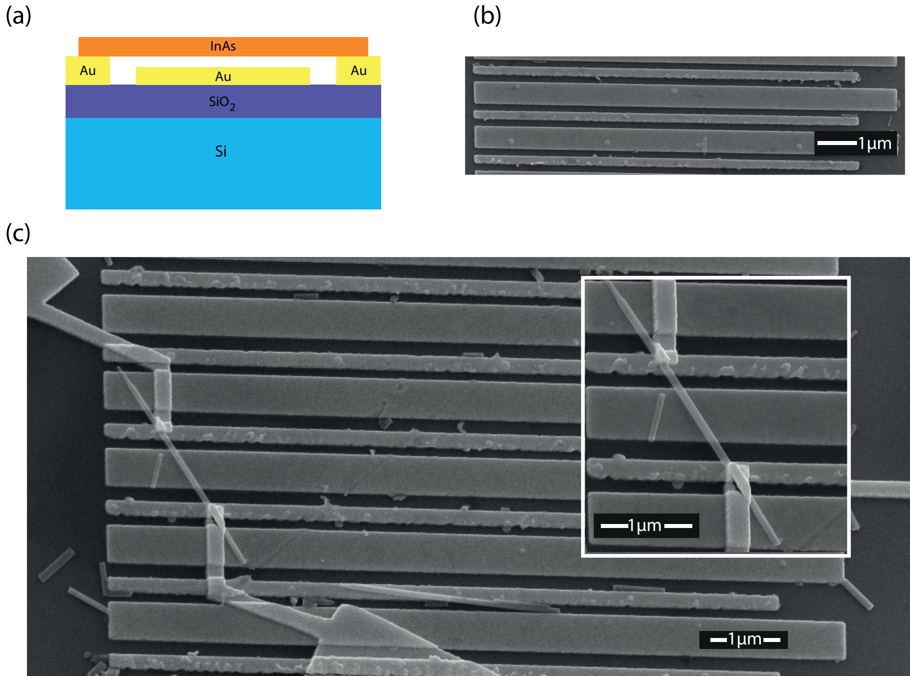

Figure 3.4: (a) Side view of suspension structure and (b) scanning electron micrograph of the fabricated structure and (c) suspended InAs device.

In order to fabricate these structures two EBL and metallization steps are required. The cleaned chips are PMMA 950 spin coated and baked with same recipe used for fabricating the source drain contacts. The source and drain stands are written by 20 kV electron beam and 10 μm

aperture size. After developing for 60 seconds in 1:3 solution of MIBK[1] in IPA it is rinsed in IPA and dried by Nitrogen Gas. 30 seconds of O_2 plasma ashing decums the patterns and 10 nm thick film of Ti and 700 nm thick layer of gold are deposited by physical vapor deposition technique. Lift-off will remove the excess metal film. The same procedure should be followed to fabricate the gate structure between source-drain stands. Only this time the gold film thickness should be 500 nm. Figure 3.4 (c) shows a suspended InAs device.

3.4 Measurement setup and metrics

In order to connect the devices to the measurement electronics, the devices are wire bonded to a measurement ceramic chip (dual inline package, DIP) by aluminium wires. Room temperature measurements are then conducted in vacuum and controlled by LabView software. Stanford SR830 has been providing the voltage sources and the current was measured by a SR570 preamplifier. All the connection cables are connected to a switching box to protect sensitive samples when changing measurement conditions.

In the following chapters a couple of important parameters are mentioned which will be explained here. In principle, the above mentioned fabricated devices are metal oxide semiconductor field effect transistors (MOSFETs) with the two contacts on the nanowire as the drain and source contacts and the gold on the back of the heavily doped silicon substrate as the gate. An important parameter in these kind of devices is transconductance which represents how the drain current at a specific drain voltage varies upon changing the gate voltage.

$$g_m = \frac{\partial I_D}{\partial V_G}|_{V_D=constant}. \tag{3.1}$$

[1] Methyl isobutyl ketone.

There are different methods to extract the threshold voltage of a MOS-FET Ortiz-Conde et al. [2002]. Here the extrapolation in the linear region method is implemented where the threshold voltage, V_T, is obtained by linear extrapolation from the maximum value of the transconductance. It is the voltage for onset of current in transistors. Figure 3.5 illustrates in schematic diagram how the threshold voltage is extrapolated.

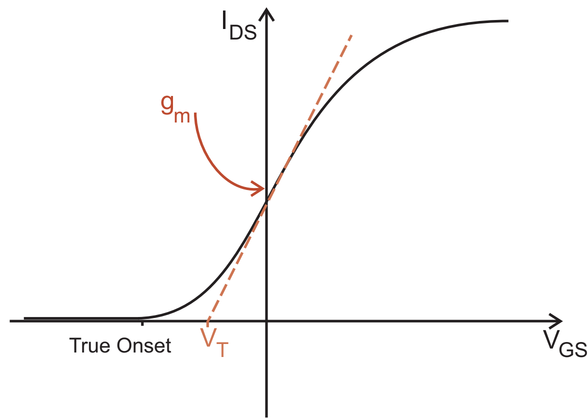

Figure 3.5: Linear extrapolation of threshold voltage implemented on $I_DS - I_GS$ characteristic at constant drain voltage. Typically the device has a true onset voltage which is different from V_T.

Chapter 4

Results

The results presented here are extracted from more than 25 different samples[1] processed with aforementioned fabrication technique. The conditions under which the measurements and fabrication processing have been carried out are kept unchanged to make sure that they do not affect the final results. For example in case of InAs nanowires all devices are processed with the same recipe mentioned in section 3.2 and measurements are carried in darkness and after 1 hour of vacuum pumping.

One of the first things that has been investigated is the possibility of any differences in characteristics of devices for which the coordinates are determined using optical microscope and scanning electron microscopy. Approximating the nanowires as a cylindrical geometry the resistivity of the nanowires are calculated by $\rho = \frac{R\pi D^2}{4L}$ where R, D and L are the nanowire resistance, diameter and length, respectively Thelander et al. [2012]. The average resistivity of the nanowires viewed using the optical microscope is 11.8 ± 2.2 mΩcm compared to the resistivity of 11.5 ± 2.2 mΩcm obtained from the nanowires viewed in scanning electron microscopy, figure 4.1. To further support this, optically aligned nanowires

[1] Each sample normally consists of 10 to 12 nanowire devices.

have been irradiated by low doses ranging from 26 to 260 μCcm^{-2} the normal dose that we used for fabricating contacts using electron beam lithography technique. Characteristics of these FET devices before and after irradiation are almost the same and there is no substantially big enough change neither in transfer characteristics nor in transconductance that suggest the effect of electron beam irradiation. Therefore, almost half of the devices are fabricated using the SEM to define the coordinates of the nanowire specially because SEM is more accurate and gives a higher yield in working devices.

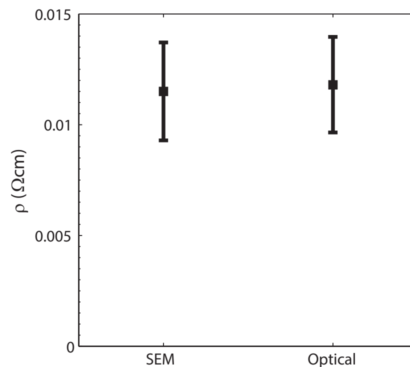

Figure 4.1: Average resistivity of the nanowires aligned with scanning electron microscopy and optical microscope.

4.1 Effect of beam energy and dose on InAs

The effects of electron beam energy and dose on InAs nanowires have been extensively studied. As illustrated in figure 3.3, three different parts of the four contact devices are defined as reference, buffer and irradiated. The reference part is to rule out the degradation of devices

over time and the buffer zone could be used to calculate the mobility of the nanowire. Having four contacts on the wire it is also possible to do four probe measurement and have an estimate of the contact resistance. The irradiated part is exposed with electrons of different energies and doses.

To begin with, the effect of dose with three different acceleration voltages is studied. Figure 4.2 shows the results for devices irradiated with different doses with electron beams of 5 kV. The dose used during the lithography of the contacts in PMMA is $260\mu\text{Ccm}^{-2}$. Irradiating the nanowires with doses lower than that has almost no discernable impact on the characteristics of nanowires; therefore, electron doses of 2.6×10^3, 2.6×10^4 and 2.6×10^5 μCcm^{-2} electrons corresponding to 10, 100 and 1000 times of the amount used for fabricating the contacts are used. The reduced resistance after irradiation of InAs nanowires with electron beam of 5 kV manifests as higher current level in figure 4.2 (c). While the resistances of the reference parts after irradiation can be rather slightly higher or lower compared to the time before, resistance of irradiated parts always has noticeably lower values, figure 4.6.

Transconductance of the wire irradiated by the highest dose of electron, $1000 \times 260\mu\text{Ccm}^{-2}$, does not have a peak value, which indicates that the drain current is hardly modified by the gate voltage. The device shows a higher off current and lower on current as compared to the time before irradiation. However, it still has slightly larger drain current at zero gate voltage which in turn give rise to its lower resistance. Linear extrapolation of current at the extracted voltage of maximum transconductance gives the threshold voltage. Table 4.1 presents the threshold voltages of irradiated parts before and after irradiation. Since the gate voltage sweep rate affects the hysteresis in the transfer characteristics Dayeh et al. [2007b] the threshold voltages are derived for both forward and backward sweeps and the gate sweeping rate is kept the same for all

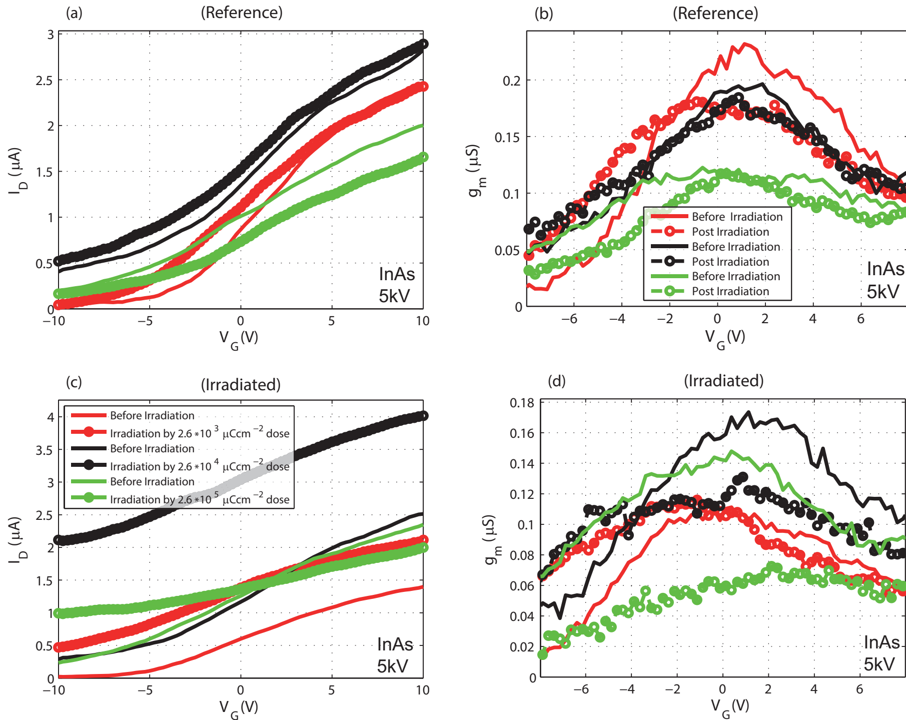

Figure 4.2: $I_D - V_G$ and transconductance of 3 different devices at $V_D = 10mV$. (a) & (b) are the transfer characteristic and transconductance of the reference parts of the nanowires before and after e-beam irradiation and (c) & (d) illustrates the same characteristics for the irradiated parts, respectively. Different colors correspond to different doses of electron.

Table 4.1: Threshold voltages for forward and backward sweeps of irradiated nanowires with 5 kV electron beam at $V_D = 10\text{mV}$.

	Forward Sweep(V)		Backward Sweep(V)	
Electron Dose ($\times 260\ \mu\text{Ccm}^{-2}$)	Before irradiation	After irradiation	Before irradiation	After irradiation
10	-7.34	-14.46	-5.42	-12.29
100	-10.06	-23.69	-6.61	-24.22
1000	-11.59	-27.46	-8.71	-19.58

of the experiments.

Figure 4.3(c) & (d) illustrate the characteristics of nanowires irradiated by beam of 10 kV and different doses. For 10 kV electron beam the lowest dose of $10 \times 260\mu\text{Ccm}^{-2}$ does not have any substantial effect on transfer characteristics. The resistance of irradiated part yet shows a higher current level at zero gate voltage and subsequently has a lower resistance. However, considering the degrading of the device over time which is indicated as a lower current level in the reference part of the same nanowire, red curves in figure 4.3 (a), and assuming that degradation is the same everywhere on the nanowire the improvement of current level in transfer characteristic is more noticeable.

The shift in the transconductances are mostly visible in 100×260 and $1000 \times 260\ \mu\text{Ccm}^{-2}$ doses can be interpreted as charging of the oxide layer in between the nanowire and heavily doped substrate. Simulation of the 10 kV beam showed that big part of the incident electrons rests inside the oxide, figures 2.2 (c) and 2.3 (b). Nevertheless, this charge is not necessarily due to irradiation. Investigation of the cap oxide charging effect due to irradiation will be discussed in suspended structure coming in the following section. The threshold voltages of irradiated part sum-

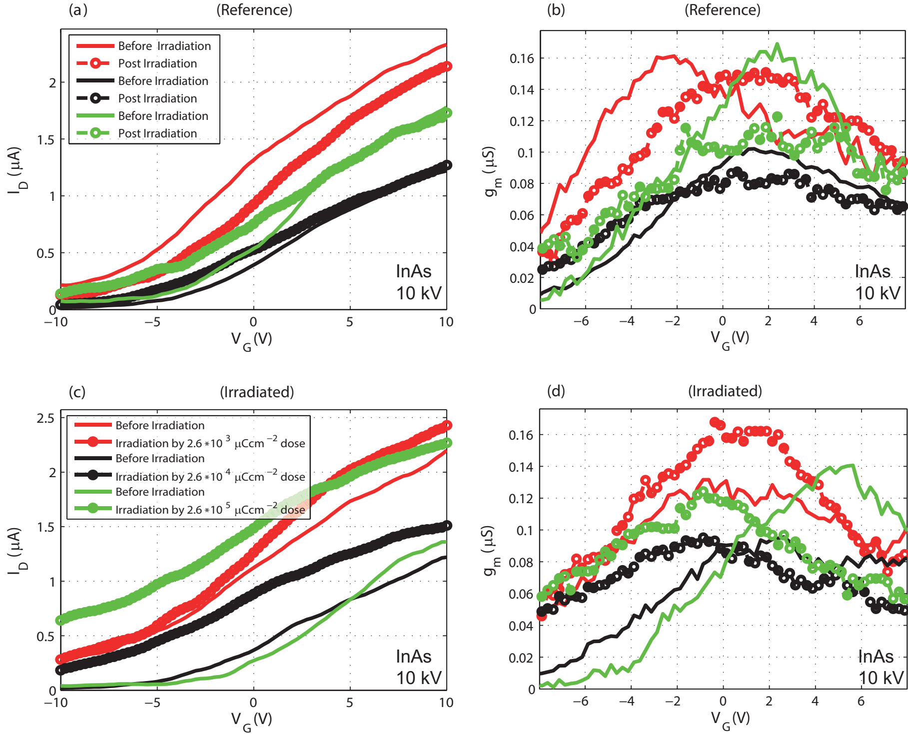

Figure 4.3: Transfer characteristics and transconductances of reference and irradiated parts of InAs nanowires with different doses of 10 kV electron beam, $V_D = 10\text{mV}$.

marized in table 4.2 move to more negative values, similar to nanowires irradiated by 5 kV beam, meaning a higher negative voltage is required to pinch-off the device.

The highest energy used to accelerate electrons for irradiation of the nanowires is 20 keV. According to the simulations, maximum penetration depth of electrons with this energy is far more than the diameter of the nanowires and electrons come to rest mostly inside the wafer. Figure 4.4 illustrates the transfer characteristics of nanowires irradiated by elec-

Table 4.2: Threshold voltages for forward and backward sweeps of irradiated nanowires with 10 kV electron beam.

Electron Dose ($\times 260\ \mu$Ccm^{-2})	Forward Sweep(V) Before irradiation	Forward Sweep(V) After irradiation	Backward Sweep(V) Before irradiation	Backward Sweep(V) After irradiation
10	-10.77	-11.02	-8.56	-7.70
100	-7.99	-12.90	-3.82	-8.99
1000	-9.36	-12.98	-0.93	-12.16

trons of 20 kV. For the lowest dose $10 \times 260\mu$Ccm^{-2} there is almost no noticeable effect on current levels and transconductances have the same peak value. However, the resistance of the irradiated part is slightly lower than before the irradiation. Furthermore, the increase of the resistance in the reference part of the same nanowire compared to its value before the irradiation suggests that the effect of irradiation is substantial and more than the general device degradation.

The threshold voltage of the wire exposed with the lowest electron dose, $10 \times 260\mu$Ccm^{-2}, is slightly shifted to more negative after irradiation whereas the wires exposed to larger doses, 100×260 and $1000 \times 260\mu$Ccm^{-2} , are shifting significantly in a negative direction. Although the device irradiated with the highest dose, $1000 \times 260\mu$Ccm^{-2}, has a very large current level improvement (lower resistance at $V_G = 0$), it shows a very weak response to the gate voltage. This weak gate response can be deduced from the almost constant value of transconductance after the device is being irradiated, green dash-circle curve in figure 4.4 (d).

Figure 4.6 shows the average of normalized resistances of different nanowires irradiated by different acceleration voltages and electron doses. It summarizes the effect of beam acceleration and dose on the resistances

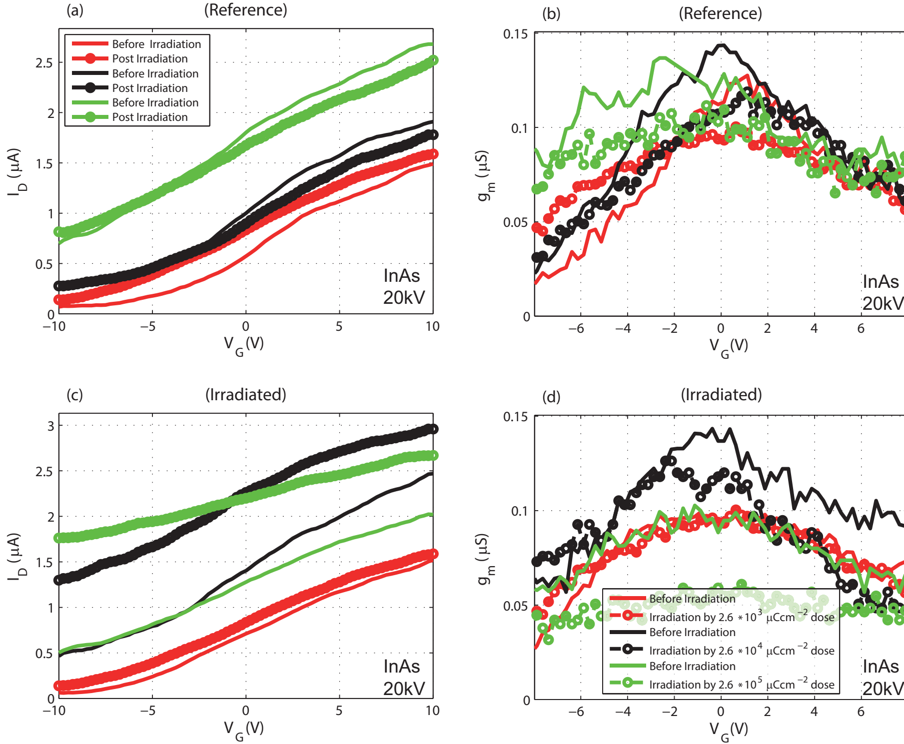

Figure 4.4: nanowires irradiated by electron beam of 20 kV at V_D = 10mV. (a) & (b) and (c) & (d) are the transfer curves and transconductances of reference and irradiated parts, respectively. Different colors correspond to different dosage of electron.

of nanowires. The average value of the reference parts of the nanowires is also plotted to show the effect of pumping and general device degradation. Upon exposure to the electron beam regardless of dosage and energy the resistance of the nanowires reduces. The average reference values for 10 and 20 kV electron beam irradiations are close to 1 compared to the average normal resistance of 5 kV which is around 1.7, figure 4.6. This might be due to lateral distribution of the backscattered elec-

Table 4.3: Threshold voltages of nanowires before and after irradiation by 20 kV beam of electron with three different doses.

Electron Dose ($\times$260 μCcm^{-2})	Forward Sweep(V) Before irradiation	Forward Sweep(V) After irradiation	Backward Sweep(V) Before irradiation	Backward Sweep(V) After irradiation
10	-11.04	-11.17	-7.10	-8.30
100	-13.56	-21.28	-10.38	-17.84
1000	-15.35	-39.40	-12.82	-41.65

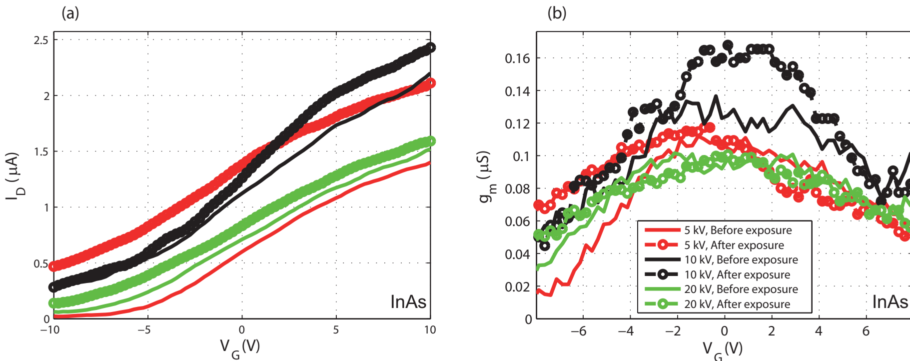

Figure 4.5: (a)Transfer characteristics and (b) corresponding transconductances of devices irradiated by $10 \times 260\mu$Ccm^{-2} dose of electron and 3 different acceleration voltages of 5, 10 and 20 kV.

trons which we believe could have affected mostly the buffer and likely the reference part of the nanowire. The reduced resistance of the buffer zone in nanowires irradiated by the highest dosage of $1000 \times 260\mu$Ccm^{-2} was clearly observed and is believed to be a direct consequence of backscattered electrons.

In order to shed light on the effect of acceleration voltage, characteris-

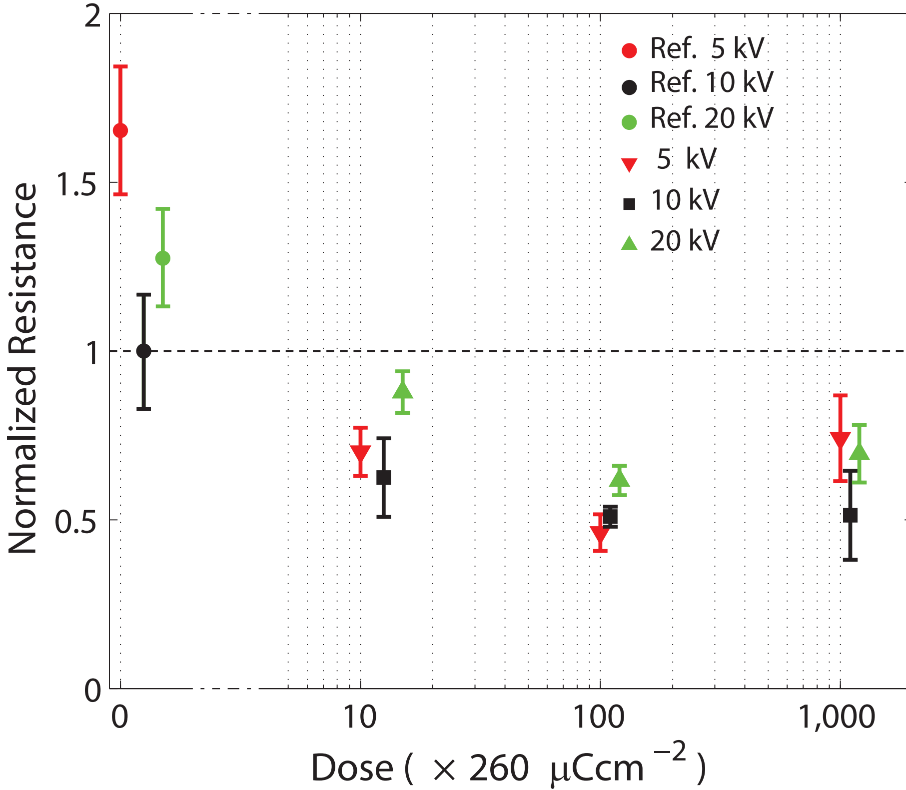

Figure 4.6: Average Normalized resistance versus the electron dose at three different acceleration voltages of 5, 10 and 20 kV. The data for 10 and 20 kV have been shifted in dose for clarity.

tic curves of devices irradiated with the same dose but different acceleration voltages are compared. Figure 4.5 plots these curves for devices irradiated by different energies but same electron dosage of $10 \times 260\mu\text{Ccm}^{-2}$. Since, according to the electron beam trajectory simulation, maximum number of electrons rest inside the nanowire for electrons accelerated to 5 kV and higher acceleration voltages of 10 and 20 have their maximum penetration depth inside the substrate, the sample irradiated by 5 kV

electron beam shows, as one might expect, the most significant impact. The drop in the resistance (minimum 6%), yet small, exists for devices exposed to 10 and 20 kV electron beams. However, the resistance drop for the 5 kV irradiated device is more significant($\approx$ 58%). Figure 4.7 also gives the same information about the effect of acceleration voltage but at higher doses of irradiation, 100×260 and $1000 \times 260\mu$Ccm^{-2}. For the dose of $100 \times 260\mu$Ccm^{-2}, figure 4.7(a-b), it is evident that higher acceleration voltages have substantial affect on the current level and increase it. For the maximum dose of $1000 \times 260\mu$Ccm^{-2} both 10 and 20 kV acceleration voltages show higher current levels compared to 5 kV. However, the transconductance is suppressed by 20 kV beam and the gate voltage does not modify the drain current as before, figure 4.7 (c-d). For the highest dose at 5 kV, although the current is higher at zero gate voltage or in another word the wire has a lower resistance, it does not respond to the gate voltage variation and has lower ON current and higher OFF current which makes it unfavorable for transistor application.

4.1.1 Charging of SiO_2 back-gate oxide

In order to investigate the effect of SiO_2 charging, a suspended structure is fabricated. The gold metal layer underneath the suspended nanowire will relinquish the possible charges introduced by irradiation. Measurements have been carried out in vacuum and darkness with the same measurement condition as above. InAs nanowires are irradiated by electron beam of 5 keV energy and doses of 10×260 and $100 \times 260\mu$Ccm^{-2} corresponding to 10 and 100 times more than what is normally used for fabricating contacts in EBL session. Figure 4.8 shows the (a) transfer characteristics and (b) the corresponding transconductances before and after irradiation. For the dose of $10 \times 260\mu$Ccm^{-2} , red and black data in figure 4.8, the current has been increased slightly and transconductances are intact. However, there is a big increase in the current level and a very

weak gate response if the wire is irradiated by $100 \times 260\mu\text{Ccm}^{-2}$ dose. Table 4.4 list resistances of nanowires before and after exposure to electron beam. Reference nanowires have shown no significant degradation in devices during the experiments.

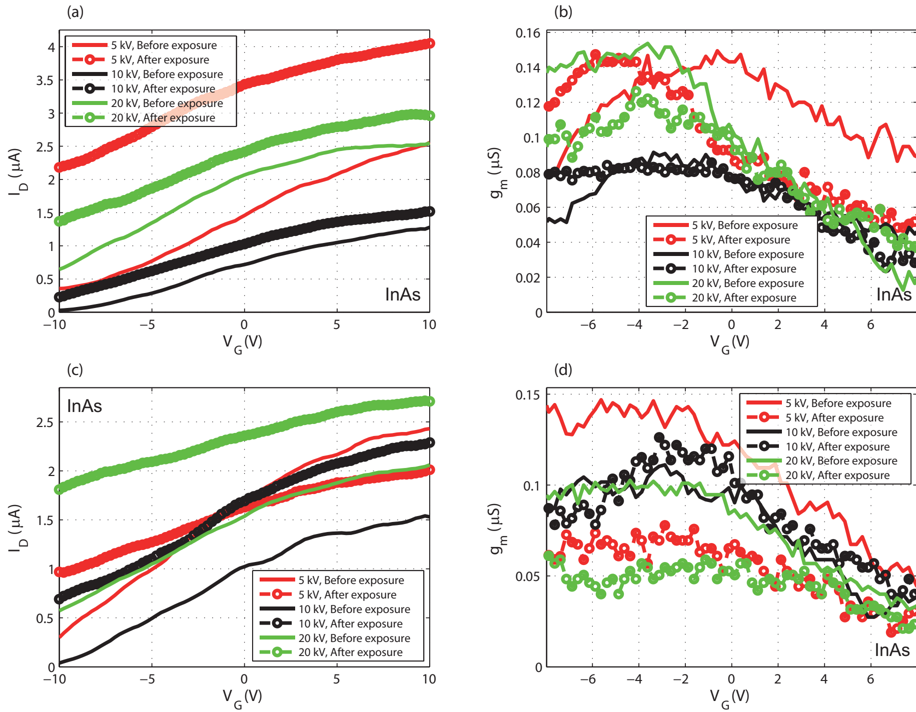

Figure 4.7: (a-b) and (c-d) correspond to transfer characteristics and transconductance plots of devices irradiated by 100×260 and $1000 \times 260\mu\text{Ccm}^{-2}$ electron doses with various acceleration voltages, respectively.

Table 4.4: Resistance and threshold voltages (only for backward sweep) of suspended InAs nanowires before and after exposure by 5 keV electron beam of doses 10×260 and $100 \times 260 \mu Ccm^{-2}$.

Electron dose	$10 (\times 260 \mu Ccm^{-2})$			
Nanowire	A		B	
	Resistance (kΩ)	Threshold voltage(V)	Resistance (kΩ)	Threshold voltage(V)
Before irradiation	39.91	-7.50	11.63	-8.86
After irradiation	38.25	-9.91	9.86	-10.87

Electron dose	$100 (\times 260 \mu Ccm^{-2})$			
Nanowire	C		D	
	Resistance (kΩ)	Threshold voltage(V)	Resistance (kΩ)	Threshold voltage(V)
Before irradiation	10.29	-13.51	10.51	-8.46
After irradiation	6.99	-58.93	6.23	-27.44

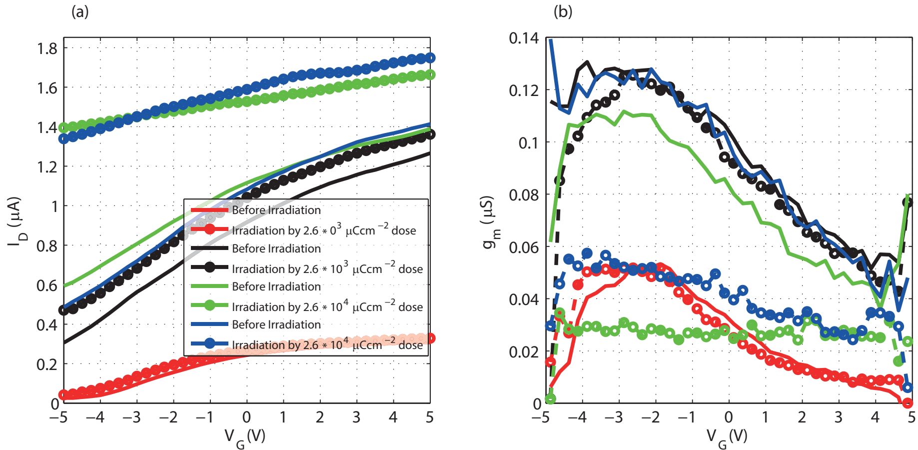

Figure 4.8: (a) $I_D - V_G$ of suspended InAs with their corresponding (b) transconductances. Transfer characteristics of color red, black, green and blue belongs to device A, B, C and D, respectively.

4.2 Irradiation of InSb

Transfer characteristics of unintentionally doped InSb nanowires representing n-type behaviour are also studied under the effect of electron beam irradiation. These wires are irradiated by electron beam of 10 kV and show similar behaviour as InAs nanowires except for very high doses of $1000 \times 260\mu\text{Ccm}^{-2}$ irradiation, for which the wires show higher resistance. Table 4.5 lists resistances of both the reference part and irradiated parts before and after irradiation. Figure 4.9 shows the transfer characteristics and the corresponding transconductances. The resistance of irradiated parts drops after exposure with both dosages of 10×260 and $100 \times 260\mu\text{Ccm}^{-2}$ however; for the highest exposure dose of $1000 \times 260\mu\text{Ccm}^{-2}$ it increases. For this dose InSb nanowires have lower current level and a very weak response to the gate voltage. Since the gate cannot modulate the current in the nanowire the transconductance does

not show any maximum value, green dash-circle line in figure 4.9 (c) & (d). Furthermore, similar to the InAs nanowires the threshold voltage of InSb nanowire FETs after electron beam exposure shift to more negative values as well. Table 4.6 lists the threshold voltages of both forward and backward sweeps before and after irradiation.

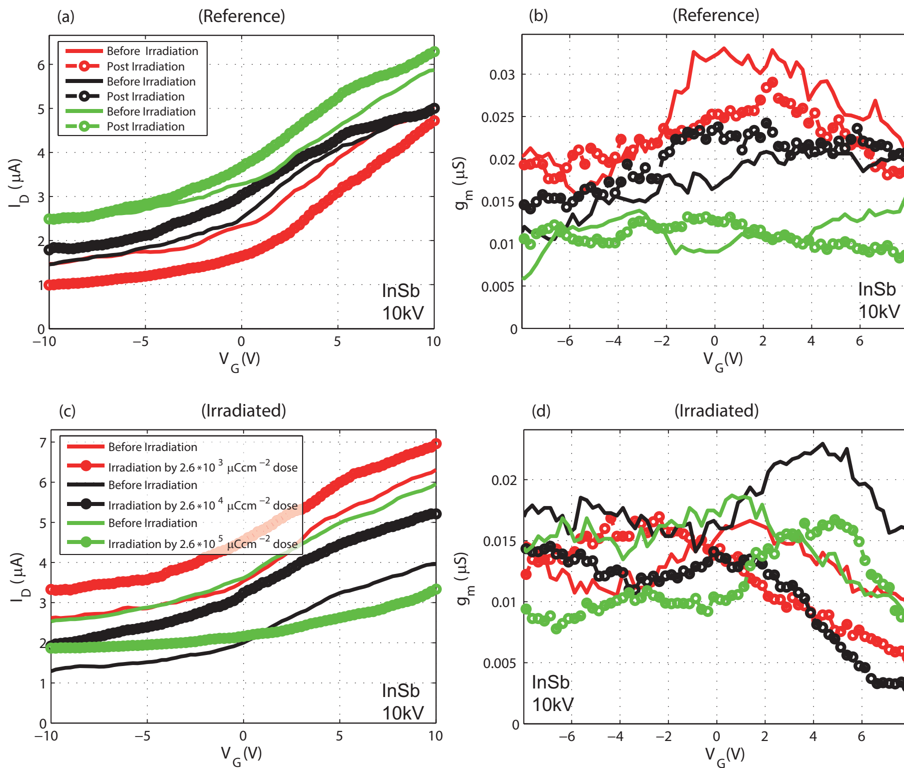

Figure 4.9: Transfer characteristics and transconductances of InSb nanowires irradiated by electron beam of 10 kV at $V_D = 25$mV with different doses of 10×260, 100×260 and $1000 \times 260\mu\text{Ccm}^{-2}$ plotted in red, black and green, respectively. (a) & (b) show the transfer curves and g_m of reference parts and (c) & (d) the transfer characteristics and g_m of irradiated parts.

Table 4.5: Resistances of the reference and the irradiated parts of the InSb nanowires before and after e-beam irradiation of 10 kV.

	Reference Part(kΩ)		Irradiated Part(kΩ)	
Electron Dose ($\times 260\ \mu \mathrm{Ccm}^{-2}$)	Before irradiation	Post irradiation	Before irradiation	After irradiation
10	8.19	11.86	4.94	4.06
100	6.76	6.04	8.46	5.88
1000	5.66	4.86	5.53	9

Table 4.6: Threshold voltages of InSb nanowires before and after irradiation by 10 kV beam of electron with three different doses 10×260, 100×260 and $1000 \times 260 \mu \mathrm{Ccm}^{-2}$.

	Forward Sweep(V)		Backward Sweep(V)	
Electron Dose ($\times 260\ \mu \mathrm{Ccm}^{-2}$)	Before irradiation	After irradiation	Before irradiation	After irradiation
10	-9.17	-18.89	-8.96	-15.50
100	-10.08	-13.58	-8.09	-13.14
1000	-14.60	-30.09	-13.25	-38.02

A corresponding increase of resistance is found in some of the InAs nanowires after being irradiated by $1000 \times 260 \mu \mathrm{Ccm}^{-2}$ dose of electron. Furthermore, after maintenance of the SEM system prolonged electron bombardment left a thick layer of carbonaceous material due to high level of organic materials inside the chamber. Figure 4.10 is an AFM image of InAs device irradiated with the highest electron dose. The step in the irradiated part of the wire is the organic layer formed.

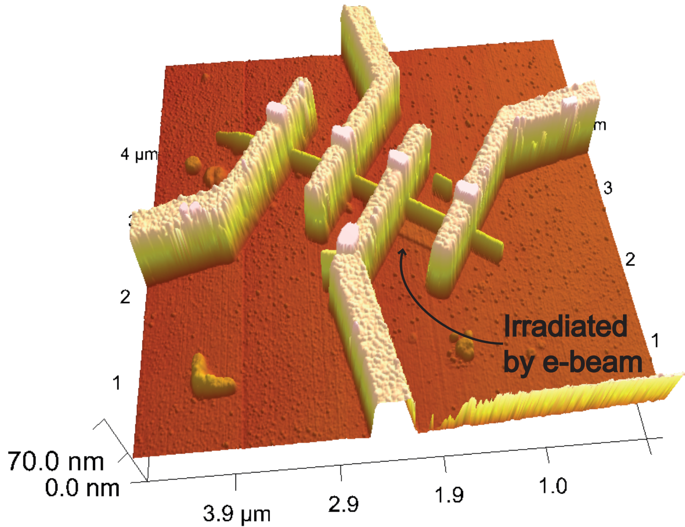

Figure 4.10: Atomic force microscopy image of InAs nanowire FET irradiated by $1000 \times 260\mu\text{Ccm}^{-2}$ electron of 5 kV. The step around the nanowire is the carbonaceous material formed by long electron exposure.

4.3 Irradiation of GaSb

GaSb nanowires were nominally used to study the effect of e-beam irradiation on a p-type material. The undoped GaSb nanowires are grown by MOVPE and show p-type behaviour. Since GaSb resistance increases upon pumping all the measurements are carried out at room temperature and pressure. A positive gate voltage depletes the nanowire at the gate interface and consequently reduces the current, figure 4.11. After exposing the nanowires by an electron beam of 10 kV and 3 different doses one can see that current levels drop which is an opposite of what

has been observed in InAs and InSb wires. Resistances of both irradiated and reference wires are listed in table 4.7. Although the drop in the resistance of the wires can also be observed in reference wires up to couple of ten kilo ohms (Maximum $\approx$ 75.5kΩ) due to degradation, the drop in the resistance of irradiated wires is far more substantial and an order of magnitude more than the reference parts for the two doses of 100 and $1000 \times 260\mu\mathrm{Ccm}^{-2}$ (Min $\approx$ 90kΩ for the lowest dose). Nevertheless, for GaSb nanowires, due to their short length, it is not possible to fabricate four contacts. Therefore, some of the nanowires have been irradiated and some are left intact as reference on each batch in order to be sure that the observed effects are due to irradiation and not general device degradation.

Table 4.7: Resistances of the reference and the irradiated parts of the GaSb nanowires before and after irradiation by 10 kV electron beam.

	Reference Part(kΩ)		Irradiated Part(kΩ)	
Electron Dose ($\times 260\ \mu\mathrm{Ccm}^{-2}$)	Before irradiation	Post irradiation	Before irradiation	After irradiation
10	95	96	155	242
100	77	83.9	162	678
1000	132.1	207.6	128	522

The threshold voltages are linearly extracted from the maximum values of transconductances, represented in figure 4.11, and are listed in table 4.8. As one can see from the transfer characteristics wires pinch-off at lower voltages after being irradiated which means that there are less carriers in the nanowire therefore; they deplete at smaller voltages. Furthermore, the effect of electron beam on intentionally p-doped GaSb nanowires has also been investigated. Due to intentional doping and

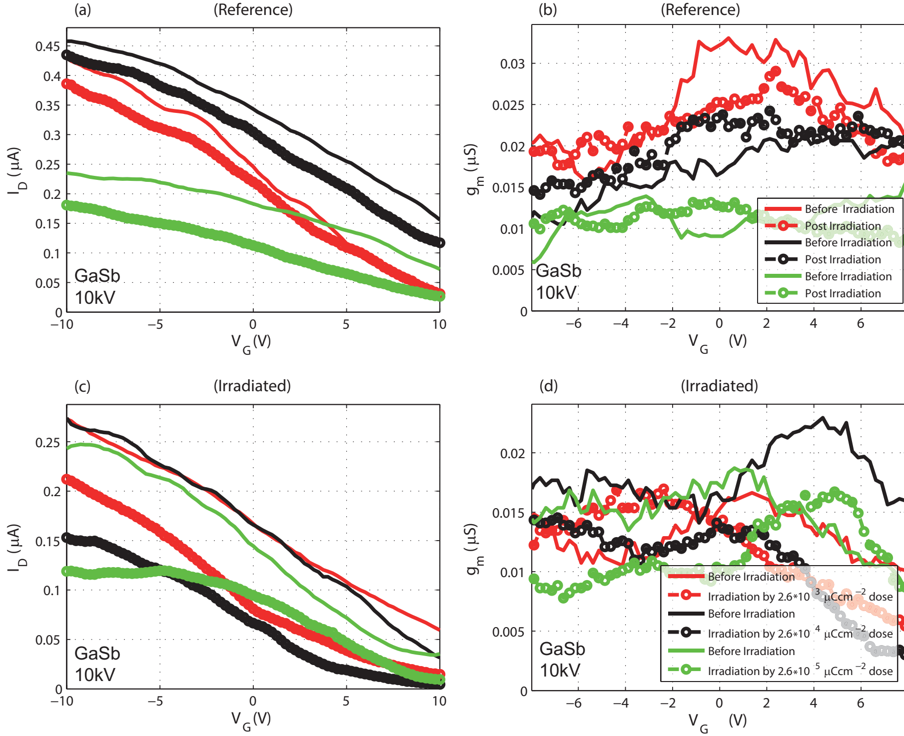

Figure 4.11: (a) and (c) are $I_D - V_G$ and (b) and (d) are $g_m - V_G$ of reference and irradiated GaSb nanowires with $V_D = 25$mV, respectively. Different doses of electron with 10 kV energy are used to irradiate the wire and are plotted in different colors.

consequently larger number of carriers, the electron beam could not affect the transport of p-doped GaSb nanowires. All fabricated devices showed almost the same behaviour before and after being irradiated by the electron beam of doses 10×260, 100×260 and $1000 \times 260\mu\text{Ccm}^{-2}$.

Table 4.8: Threshold voltages of GaSb nanowires before and after irradiation by 10 kV beam of electron determined by linear extrapolation from the voltage corresponding to the maximum of transconductance plotted in figure 4.11 (d).

Electron Dose ($\times 260\ \mu C cm^{-2}$)	Forward Sweep(V) Before irradiation	Forward Sweep(V) After irradiation	Backward Sweep(V) Before irradiation	Backward Sweep(V) After irradiation
10	10.30	3.64	14.12	5.12
100	4.41	-0.40	13.18	5.65
1000	4.35	-3.85	8.80	9.62

Chapter 5

Discussion and Outlook

The scope of the thesis covers the investigation of the effects of electron beam exposure on the transport properties of mainly InAs and partially InSb and GaSb nanowires, during which fabrication and characterization of these nanowires are learned. It is shown that the electrical conductance of undoped InAs and InSb nanowires (n-type) are enhanced upon being exposed to electron beam of various doses and energies. However, irradiation of the unintentionally doped p-type GaSb nanowires reduces their conductances. In addition, performing the measurement in air or vacuum shows that regardless of electron beam exposure InAs and InSb nanowires show higher resistances in air but GaSb the opposite. The results are interpreted by the desorption of polarized water molecules or oxygen ions from the surface in vacuum. The increase of the current in InAs nanowires in vacuum can be discussed in terms of detachment of polarized water molecules and oxygen ions which are weakly adsorbed (physisorbed) to the surface and are sources of screening charges. Due to dipole nature of water molecules they can be adsorbed from different orientation canceling charge carriers on the surface. On the contrary, detachment of an oxygen ion with negative charge would have opposite effect on the conductance of n-type and p-type materials by releasing an

electron. Since the opposite tendency in conduction is observed in n-type InAs and InSb and p-type GaSb nanowires after pumping, it can be inferred that desorption of the oxygen ions in GaSb is more important than polarized water molecules. Thus, it is a competitive mechanism and carrier concentration (holes) in GaSb reduces due to compensation of released electrons with holes. Figure 5.1 illustrates the adsorption and desorption of oxygen and water molecules during the 4 different stages of measurement according to explanation proposed for oxide nanowires Ji et al. [2011]. However, our observation for p-type III-V nanowires of GaSb is not fully consistent with observations in the case of oxide nanowires.

According to Akamatsu et al. [1998] the electron beam irradiation of InAs can affect the etching rate of its native oxide by Cl_2. For low dose, electron beam has positive effect on the Cl_2 etching rate which means that the irradiated surface is etched more than the non-irradiated areas. The effect of the beam on the etch rate depends both on the beam energy and the exposure dose. Lower energy beam is found to be more effective. Furthermore, results show that the negative effect occurs if electron doses higher than $4.8 \times 10^3 \mu\text{Ccm}^{-2}$ and $3.2 \times 10^5 \mu\text{Ccm}^{-2}$ are used at energies of 5 and 20 keV, respectively Akamatsu et al. [1998]. The electron beam is believed to locally modify the chemical bonds at the irradiated area by transferring heat and cause exodiffusion of oxygen generating In-In bonds or In precipitates at the surface Akamatsu et al. [1998], which makes it easier for Cl_2 to etch.

Based on our observed results from nanowires irradiated by electron beam and in line with the Akamatsu et al. [1998] findings on Cl_2 etching rate of InAs native oxide, the increased conductance in InAs and InSb nanowires after irradiation can likely be related to detachment of oxygen ions from the surface. The possible exodiffusion of oxygens and modified bonds on the surface of the nanowire, due to electron beam exposure, re-

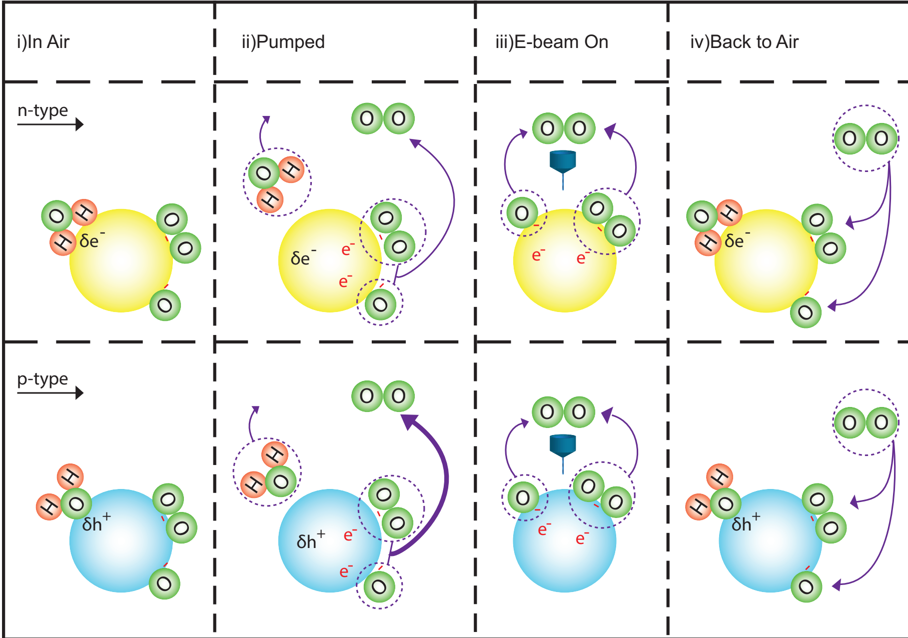

Figure 5.1: Schematic illustration of adsorption and desorption of oxygen and water molecules based on the explanation proposed for oxide nanowires Ji et al. [2011] on the surface of n-type and p-type nanowires at different steps of measurement:(i) in air, (ii) in evacuation, (iii) in evacuation chamber of SEM for irradiation and (iv) back to the air again.

sults in formation of a different oxide layer after the sample is re-exposed to air. Modified oxide might lead to different charging states of the vacancies and can be responsible for the increase of current after irradiation. In addition, the exodiffusion of oxygen in GaSb due to electron beam irradiation, releases electrons in GaSb which then compensates the number of holes and decreases the hole concentration. After irradiation when the sample is exposed to air, oxygen and water molecules are reabsorbed reconstructing crystallographic of the surface. Since GaSb is a

p-type material, decrease in current shows lower carrier concentrations, which might be due to formation of new oxide layer. Electron beam irradiation effects in oxide nanowires have also been studied and are in good agreement with our hypothesis Ji et al. [2011].

There are still questions that needs to be addressed about the effect of electron beam on different semiconductor nanowire materials. Below we summarize some of the main ideas and experiments that can be carried out in order to better understand the phenomenon:

- The electrical properties of the irradiated nanowires can be studied after etching the native oxide by ammonium hydroxide NH_4OH to see if the formation of a new oxide layer has any effect in eliminating the impact of electron beam exposure.

- Carrying out in-situ measurements inside the SEM and also controlling the pressure in order to verify the effect of ambient air and humidity on the electrical properties.

- In-situ irradiation of nanowires inside the growth chamber directly after growth by electron beam (possible by reflection high energy electron diffraction (RHEED) System in Chemical beam epitaxy (CBE)) to eliminate the effect of native oxides.

- Atomic hydrogen cleaning in ultra high vacuum can be used to etch the surface and remove the oxide layer.

- The different conductances of the GaSb nanowires in air and after pumping can be investigated in a controlled way for possible sensor applications, most probably oxygen or humidity sensors.

- Scanning tunnelling microscopy of the nanowire surface to investigate possible surface structure and likely surface modifications after electron beam irradiation.

Appendix A

Reference Chips Fabrication

In this appendix processing of the reference chips is described in details. Fabricating the reference chips requires electron beam lithography, UV lithography, physical vapor epitaxy, spin coating and lift off. This process commence with cleaning a 2 inch Si wafer. The cleaning process is simply rinsing the wafer into Acetone and using sonic bath in order to remove any particles or dirts from the surface. Next, wafer is submerged into IPA after which it is blown dry by Nitrogen. Acetone is a typical solvent for most plastics and synthetic fibers while IPA dissolves a wide range of non-polar compounds and is widely used as a cleaning fluid. After cleaning the substrate with Acetone and IPA the wafer is left on a hot plate at 100 ℃ for 1 minute to make sure all the fluid residues are evaporated and we have a clean dry substrate.

A.1 First metallization

Now that the wafer is clean the capped surface is spin coated with the photo resist S1813[1] and baked at 115 ℃ for protecting its nice and clean surface. Due to exposure to the air the back side of the wafer oxidizes. Hydrofluoric acid buffered with Ammonium Fluoride (BHF) is used to remove the silicone oxide. The wafer is placed in a teflon or high density polypropylene watch glass coated side down and hydrofluoric acid is poured by a pipette to cover the back side. The HF will reacts with the SiO_2 forming a Hexafluorosilicic acid H_2SiF_6 and water. The hexafluorosilicic acid is water soluble and leaves the surface of the wafer. After removing the oxide layer the sample is placed in an evaporation system to deposit 10 nm of titanium and 100 nm of gold. The titanium layer is used as an sticking layer since gold does not stick to silicon very well.

A.2 EBL step and second metallization

To create the nanometer size patterns on the chips electron beam lithography step is required. The protective resist layer on the top is removed by Remover 1165[2] to instead spin coat it by a high resolution electron beam sensitive resist, ZEP 520A7, at the spin speed of 6000 rpm for 2 minutes. According to the ZEP 520A7 data sheet[3] the final thickness of the film should be around 1800 Å. It is then baked at 180 ℃ for 10 minutes. The pattern which is transferred into the wafer in this step is highlighted in figure 3.1. Recommended doses for 5 kV acceleration voltage and 10μm in Raith150 EBL system is listed in table A.1. This step is very time consuming and is normally done in an overnight time

[1] Mico Chem Corporation, Newton, MA, USA.
[2] Micropoit Remover 1165, Shipley Company, Marlboro, MA, USA.
[3] Zeon Corporation, Tokyo, Japan.

Table A.1: Recommended doses for electron beam lithography pattern using 5 kV and 10 μm aperture size in Raith150.

	Dose	Step size
Area Dose (μCcm^{-2})	20	30 nm
Line Dose ($pCcm^{-1}$)	120	2 nm
Dot Dose (pC)	0.007	-

slot. The mechanism behind this technique is that the beam of electrons scissors polymer chains in the resist which allows the exposed parts to be removed by appropriate developer. Oxylene is a standard developer for ZEP. An oxygen plasma ashing is the following processing step used to etch away layers of the photo resist film remained on the developed parts. Besides, it removes organic materials and compositions, carbon oxides and water from the surface. Finally the metallization is carried out by depositing 3 nm of titanium and 30 nm of gold. Lift-off is performed in heated remover 1165.

A.3 UV lithography and third metallization

To connect the nanometer world to the macroscopic world micrometer sized metal pads are fabricated by the use of UV lithography. The obstacle here is aligning the nanometer size patterns with the mask in the mask aligner. Figure A.1 illustrates the micrometer metal pads well aligned with the nanometer size patterns. Before using the mask aligner the wafer needs to be spin coated with LOR7B, the undercut layer, and S1318, the photoresist. LOR is a polydimethylglutarimide based resist which can be used either as a sacrificial layer or undercut layer in bi layer lift-off processes. It has a very good adhesion to wide range of semiconductors. The LOR7B has been spin coated on the sample with spin speed

of 5000 rpms for 1 minute to have a thickness of roughly 6000 Å. It is then baked in the oven at 180 ℃ for 20 minutes or on hot plate at 165 for 5 minutes to fix the development and undercut rate and primarily drying the LOR film.[1] S1813 which is a microcomposite (positive) photoresist sensitive to light sources with spectral range of 350nm to 450 nm is then used to cover the LOR layer by spin speed of 5000 rpm for 1 minute. This spin speed will leave a roughly 12000Å thick layer of positive photo resist on the LOR layer creating a bilayer lift-off coat. The substrate is then baked at 115 ℃ for 90 seconds. An ultra violet mask aligner in hard contact mode should be used to transfer the patterns on the mask to the photo resist on the substrate with the highest possible procession. The 365 nm light source on the mask aligner exposes the resist layer of S1813. After developing the sample for 45 seconds in MF-319[2] developer and rinse in water for 30 seconds one can inspect the transferred pattern on the resist. Since a positive photo resist has been used, the exposed areas can be easily removed in the development process.

Oxygen plasma ashing should again be carried out to make sure that no resist is left in the developed parts. The final metallization is evaporating 5 nm of titanium as a sticking layer followed by 100 nm of gold. Lifting off the exceeding metals are simply done in heated Acetone. The process is finished by scribing the wafer into small chips approximately $4mm \times 6mm$ in size using a diamond tipped scriber.

[1] Mico Chem Corporation, Newton, MA, USA.
[2] Shipley Company, Marlborough, MA, USA.

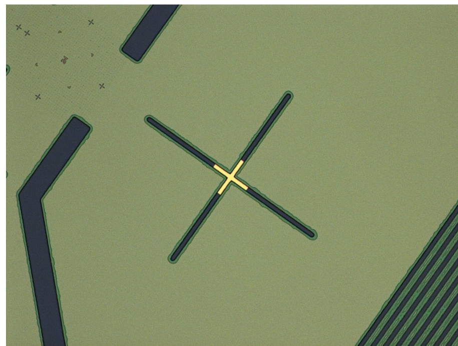

Figure A.1: Optical microscope image of perfectly aligned micrometer size UV lithography pattern with already fabricated EBL patterns. The contrast around the developed area shows the undercut.

References

B. Akamatsu, P. Henoc, S. Miya, and H. Sakaki. Effect of electron beam irradiation followed by thermal etching on InAs substrate. *The European Physical Journal Applied Physics*, 2:151–155, 1998. 2, 49

H. U. Baier, L. Koenders, and W. Monch. Oxidation of cleaved InAs (110) surface at room temperature : surface band-bending and ionization energy. *Solid State Communications*, 58(5):327–331, 1986. 1

Yi Cui, Qingqiao Wei, Hongkun Park, and Charles M. Lieber. Nanowire nanosensors for highly sensitive and selective detection of biological and chemical species. *Science*, 293:1289– 1292, 2001. 1

Shadi A. Dayeh, David P. R. Aplin, Xiaotian Zhou, Paul K. L. Yu, Edward T. Yu, and Deli Wang. High electron mobility InAs nanowire feild effect transistors. *Small*, 3(2):326 332, 2007a. 1

Shadi A. Dayeh, Cesare Soci, Paul K. L. Yu, Edward T. Yu, and Deli Wang. Transport properties of InAs nanowires field effect transistors : The effects of surface states. *Journal of Vaccum Science Technology B*, 25(4):1432–1436, 2007b. 30

Hendrix Demers, Nicolas Poirier-Demers, Alexandre Real Couture, Dany Joly, Marc Guilmain, Niels de Jonge, and Dominique Drouin. Three-

dimensional electron microscopy simulation with CASINO monte carlo software. *Scanning*, 33(3):135–146, 2011. 11

Dominique Drouin, Alexandre Real Couture, Dany Joly, Xavier Tastet, Vincent Aimez, and Rynald Gauvin. CASINO V.2.42- a fast and easy-to-use modeling tool for scanning electron microscopy and microanalysis users. *Scanning*, 29(3):92–101, 2007. 9

R. F. Egerton, P. Li, and M. Malac. Radiation damage in the TEM and SEM. *Micron*, 35:399–409, 2004. 2, 5

S. V. Eremeev, N. A. Valisheva, O. E. Tereshchenko, and S. E. Kulkova. Change in the electronic properties of an InAs (111)A surface at oxygen and fluorine adsorption. *Semiconductors*, 46:4955, 2012. 1

Youfan Hu, Jun Zhou, Ping-Hung Yeh, Zhou Li, Te-Yu Wei, and Zhong Lin Wang. Supersensitive, fast-response nanowire sensors by using schottky contacts. *Advanced Materials*, 22:3327–3332, 2010. 1

Hyunjin Ji, Jaewan Choi, Youngseung Cho, In-Sung Hwang, Sun-Jung Kim, Jong-Heun Lee, Siegmar Roth, and Gyu-Tae Kim. Electron beam tuning of carrier concentrations in oxide nanowires. *Journal of Applied Physics*, 110:013705, 2011. ix, 1, 49, 50, 51

Charels Kittel. *Introduction to Solid State Physics*. John Wiley & son, NJ, 2005. 2, 16

Yat Li, Fang Qian, Jie Xiang, and Charles M. Lieber. Nanowire electronic and optoelectronic devices. *Materialtoday*, 9(10):18–27, 2006. 1

Gabriel P. Lopez, Hans A. Biebuyck, and George M. Whitesides. Scanning electron microscopy can form images of patterns in self-assembly monolayers. *Langmuir*, 9:1513–1516, 1993. 2, 5, 9

Marc J. Madou and Stanley Roy Morrison. *Chemical sensing with solid state devices.* Academic Press, Boston, 1989. 13

A. Melchinger and S. Hofmann. Dynamic double layer model: Description of timer dependent charging phenomena in insulators under electron beam irradiation. *Journal of Applied Physics*, 78(10):6224–6232, 1995. 2, 7, 8

Winfried Monch. *Semiconductor surfaces and interfaces.* Springer-Verlag, Berlin, 2010. 13

A. Ortiz-Conde, F.J. Garcia Sanchez, J.J. Liou, A. Cerdeira, M. Estrada, and Y. Yue. A review of recent MOSFET threshold voltage extraction methods. *Microelectronics Reliability*, 42:583596, 2002. 27

M. Prutton. *Surface Physics.* Oxford University Press, London, 1975. vii, 13, 15, 16

E.I. Rau, E. N. Evstaf'eva, and M. V. Andrianov. Mechanism of charging of insulators under irradiation with medium-energy electron beam. *Physics of the Solid state*, 50(4):621–630, 2008. vi, 2, 8, 9

H. Seiler. Secondary electron emission in the scanning electron microscope. *J. Appl. Phys.*, 54(11):R1–R18, 1983. 5

K. Smit, L. Koenders, and W. Mnch. Adsorption of chlorine and oxygen on cleaved InAs(110) surfaces: Raman spectroscopy, photoemission spectroscopy, and kelvin probe measurements. *Journal of Vacuum Science & Technology B*, 7(4):888, 1989. 1

S. M. Sze. *Semiconductor devices, Physics and Technology.* John Wiley & son, New York, 1985. vii, 17

C. Thelander, M.T. Bjork, M.W. Larsson, A. E. Hansen, L. R. Wallenberg, and L. Samuelson. Electron transport in InAs nanowires and

heterostructure nanowire devices. *Solid State Communications*, 131: 573–579, 2004. 22

Claes Thelander, Philipe Caroff, Sebastien Plissard, and Kimberly A. Dick. Electerical properties of $InAs_{1-x}Sb_x$ and InSb nanowires grown by molecular beam epitaxy. *Applied Physics Letters*, 100:232105, 2012. 28

R. K. Willardson and Albert C. Beer. *Semiconductors and Semimetals*, volume 4. Academic Press, New York & London, 1986. 2

Ruoxue Yan, Daniel Gargas, and Peidong Yang. Nanowire photonics. *Nature Photonics*, 3:569–576, 2009. 1